Human Remains from Areas C and D: Morphological and Palaeopathological Investigations

Julia Gresky

Introduction

The Neolithic Levant is a key area for bioarchaeological studies investigating the impact of new life styles on human health. This region witnessed the transition to agriculture and sedentism as one of the earliest in the world (Simmons 2007). After a slow start of bioarchaeological and in particular palaeopathological research in the Levant (Smith *et al.* 1984 with further references; Shewan 2004; Perry 2012 with further references), a lot of new studies on human remains from Neolithic sites have been published within the last decades. They comprise population dynamics, foodways, and mobility (*e.g.*, Balasse *et al.* 2014; Itahashi *et al.* 2018; Feldman *et al.* 2019; Santana *et al.* 2021; Wang *et al.* 2023; Knipper this volume, Skourtanioti and Feldman this volume), and the emergence and spread of infectious diseases like tuberculosis (Hershkovitz *et al.* 2008; Baker *et al.* 2015) using isotopic and genetic analyses. Furthermore, the examination of non-metric traits in skeletons has provided insights into social interactions among Neolithic communities during the transition to larger settlements (Alt *et al.* 2013, 2015). Bioarchaeological and palaeopathological studies in Neolithic Jordan have predominantly focused on assessing the general health status of the buried group or presenting interesting single cases. Notable examples include ‘Ain Ghazal (El-Najjar *et al.* 1996), Ba`ja (Schultz *et al.* 2004, 2007; Benz *et al.* 2019, 2020, 2023, this volume Part 2), Basta (Schultz *et al.* 2004, 2007), Shkārat Msaied (Hermansen *et al.* 2006; Kinzel *et al.* 2017).

Large scale palaeopathological investigations to answer questions of subsistence strategies or the impact of sedentism on human health pose significant difficulties. These challenges primarily arise from the limited accessibility to excavated skeletons and their generally poor state of preservation. It is further complicated by the specific burial customs, which often include commingled remains in multiple burials or secondary burials, *e.g.*, missing skulls (*e.g.*, Hermansen *et al.* 2006; Schultz *et al.* 2007; Kinzel *et al.* 2017). Until large scale excavations of burial sites will produce relevant numbers of individuals, we could contribute to collect data on health in Neolithic Jordan by publishing standardised data of our skeletal collections, even if small, to provide comparative data for future analyses. This will allow a *longue durée* perspective on people’s life in the Near East (Perry 2012; Schultz and Schultz 2019).

Presenting the osteological and palaeopathological analyses of 16 individuals of single and double burials is the first step to publish results of the analyses of the human remains from Ba`ja. The publications of the human skeletal remains from four collective burials and a female single burial are in preparation. All available data will be provided for comparative analyses (see Appendix 1 for the catalogue). To avoid excessive diagnosing, this contribution is rather descriptive. While acknowledging the limited number of available data, we would like to address the question whether the health status of individuals and burial customs in Ba`ja are similar when compared to other Neolithic sites in the Levant. Krauß *et al.* present non-metric traits of human teeth in this volume.

Materials

The human skeletal remains that are presented in this contribution were excavated in Ba`ja in 2016, 2018, and 2019. They include mainly skeletons of infants and children, with only a few exceptions. Detailed descriptions of the burial contexts and processes can be found in Benz *et al*. this volume, Part 2. This

Benz M., Gresky J., Purschwitz C. and Gebel H.G.K. (eds.), *Death in Ba`ja. Sepulchral Identity and Symbolism in an Early Neolithic Community of the Transjordanian Highlands. Household and Death in Ba`ja* 2.
bibliotheca neolithica Asiae meridionalis et occidentalis. 2023. Berlin: ex oriente.
DOI: https://doi.org/10.11588/propylaeum.1224.c19494

Table 1 Ten burials comprising 16 individuals were found in Areas C and D during the excavation seasons 2016, 2018, and 2019. LM = lunar month. Sex estimation relies on cranial features, only individual Loc. C10:405-I was genetically identified as female.

Year of Excavation	Room	Locus	Grave Number	Age at Death	Sex	Burial Type
2016	CR35	C10:408.8	CG10	25-35 years	m>=f	single
2016	CR35	C10:405, Ind. I	CG8	6-9 months	f (genetic)	double
2016	CR35	C10:405, Ind. II	CG8	3-4 years	m=f	double
2018	CR36.1	C1:46	CG7	8 years (± 24 months)	f>>m	single
2019	CR6	CR6:23a	CG5	3 years (± 12 months)	m=f	double
2019	CR6	CR6:23b	CG5	1.5-2 years	m=f	double
2019	CR6	CR6:40	CG6	0 years (± 2 months)	m=f	single
2019	CR6	CR6:48	CG4	7 years (± 24 months)	f>=m	single
2019	DR19	DR19:110	DG2	0 years	m=f	single
2019	CR5	CR5:49A	CG3	1.5-2 years	m=f	single
2019	CR5	CR5:53	CG2	4 years (+ 12 months)	f>m	double
2019	CR5	CR5:54	CG2	18 months	m=f	double
2019	CR28.2	CR28.2:122a	CG9	3 years (+ 12 months)	m=f	multiple
2019	CR28.2	CR28.2:122b	CG9	3 years (± 12 months)	m=f	multiple
2019	CR28.2	CR28.2:123a	CG9	9.5 LM	m=f	multiple
2019	CR28.2	CR28.2:123b	CG9	9.5-10 LM	m=f	multiple

contribution is based on ten burials containing a total of 16 inhumations (Table 1).

The preservation of the human bones was very poor (Table 2). Particularly, their consistency was extremely brittle. The bones were already fragmented upon exposure, which made their excavation very challenging. Although they had been packed bone by bone during the excavation, extensive restoration in the laboratory was necessary to reassemble the fragments (Fig. 1). The degree of fragmentation seems to be dependent on the size of the bone: the smaller a bone is, the less fragmented it appears, *e.g.*, infant bones (Fig. 2) were much better preserved than the large bones of adult skeletons (Fig. 3). This correlation might be due to soil pressure which particularly affects larger bones.

Fig. 1 Overview of the bones and bone fragments of the multiple infant Burial CG9, Room CR28.2, in the lab. (Photo: J. Gresky, Ba`ja N.P., DAI)

Fig. 2 Well-represented and preserved skeleton of the newborn of Burial CG6, Loc. CR6:40. (Photo: J. Gresky, Ba`ja N.P., DAI)

Table 2 All skeletons and additional bones with their representation (repr.) in % of the whole skeleton, their preservation (ranging from relatively solid to very fragile), and the surface composition (ranging from good to severely eroded). For a better comparison of the factors to age groups, they were combined to five classes: around birth, younger and older infants, child and adult.

Room	Locus	Age	Repr. (%)	Preservation			Surfaces			
				solid	fragile	very fragile	good	moderate	eroded	severely eroded
CR35	C10:408.8	adult	5			1				1
CR35	C10:405-I	around birth	90		1			1		
CR35	C10:405-II	older infant	80			1		1		
CR36.1	C1:46	child	40			1				1
CR6	CR6:23a	older infant	40		1				1	
CR6	CR6:23b	younger infant	30			1			1	
CR6	CR6:40	around birth	100	1			1			
CR6	CR6:41a	adult	1		1					1
CR6	CR6:41b and c	around birth	1	1					1	
CR6	CR6:48	child	90			1			1	
DR19	DR19:110	around birth	80		1		1			
CR5	CR5:49A	younger infant	5			1				1
CR5	CR5:54	younger infant	10		1		1			
CR5	CR5:53	older infant	50			1				1
CR28.2	CR28.2:122a	older infant	30			1				1
CR28.2	CR28.2:122b	older infant	5			1				1
CR28.2	CR28.2:123a	around birth	35			1				1
CR28.2	CR28.2:123b	around birth	35			1				1

Fig. 3 Highly fragmented long bones of the adult male of CG10, Loc. C10:408.8. (Photo: J. Gresky, Ba`ja N.P., DAI)

The surfaces of the bones showed different states of preservation. In the multiple infant Burial CG9, Loci CR28.2:122a-b/123a-b, the severe erosion resulted in the complete absence of the original bone surfaces. The bones were reduced to a thin layer of the former original bones, causing a disproportionately thinned cortical bone compared to its normal size. In other burials, *e.g.*, CG6, Loc. CR6:40, the surfaces were much better preserved (Fig. 1) so that it was possible to examine them for pathological processes.

Macroscopically visible taphonomic alterations could be detected such as the presence of red staining on bones from Burial CG5, Loc. CR6:23a-b (Fig. 4); CG7, Loc. C1:46 (Figs. 5, 6) (Reifarth *et al.* this volume), and to a lesser degree on Burial CG2, Loc. CR5:54 (Fig. 7), as well as dark spots on the surfaces of bones of many skeletons (Table 3), *e.g.*, from the burials CG7, Loc. C1:46 (Fig. 5) and CG2, Loc. CR5:54 (Figs. 7, 15). This might be due to the manganese content of the soil (*e.g.*, López-González *et al.* 2006). Erosion of the surfaces by plant roots was evident for example in CG2, Loc. CR5:53 (Fig. 8) and particularly severe in the bones of the adult male in CG10, Loc. C10:408.8 (Fig. 9). There was no evidence of carnivore bite marks. Gnawing marks

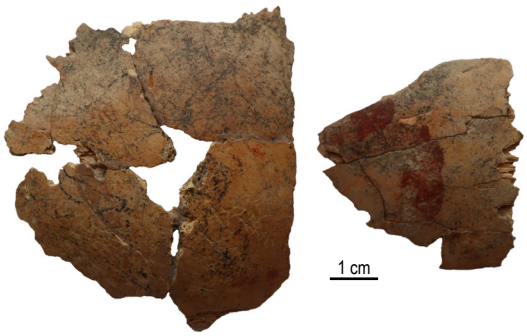

Fig. 4 External lamina of the right parietal bone of CG5, Loc. CR6:23a with localised large red colouring in the anterior part (right in the picture). (Photo: J. Gresky, Ba`ja N.P., DAI)

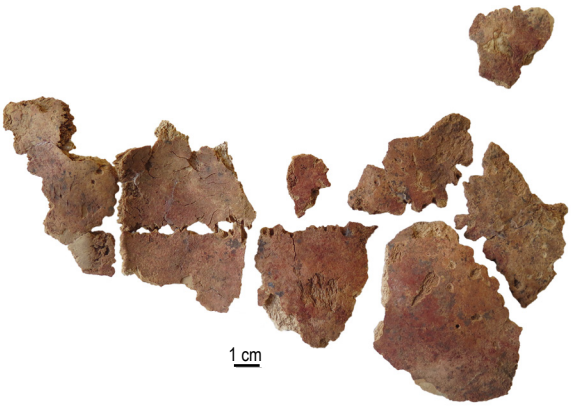

Fig. 5 View of the external lamina of the superior region of the frontal, both parietal, and occipital bones of CG7, Loc. C1:46 with equally distributed red staining. (Photo: J. Gresky, Ba`ja N.P., DAI)

Fig. 6 Anterior view of the bones of the left arm (from top to bottom: humerus, radius, ulna) of CG7, Loc. C1:46 with slight equally distributed red staining. (Photo: J. Gresky, Ba`ja N.P., DAI)

Fig. 7 Anterior view of the right frontal of CG2, Loc. CR5:54 with several small red spots. (Photo: J. Gresky, Ba`ja N.P., DAI)

Fig. 8 Dorsal view of the left parietal bone of CG2, Loc. CR5:53 with distinct plant root etching. (Photo: J. Gresky, Ba`ja N.P., DAI)

of rodents could only be detected on bones from Burial CG10, Loc. C10:408.8 (Fig. 10) and in one adult rib fragment (Loc. CR6:41a), which belonged to isolated additional bones in Burial CG6.

Methods

After excavation, the bones were dry cleaned in the laboratory, and the fragments were then glued with *Ponal*©, a water-soluble wood glue.

All bones underwent macroscopic examination with a magnifying glass (8-10x magnification). Detailed analyses of surface changes were conducted using the digital microscope *Hirox KH-870031* with magnifications ranging from 20 to 160 times.

All skeletons were subjected to plain radiography, if their state of preservation allowed for it. They were radiographed in anterior-posterior and lateral beam path with the *Faxitron 43805N* by *Hewlett Packard* using 60-80kV, 3mAs.

Sex determination was based on cranial and pelvic morphology using anthropological standards (Phenice 1969; Acsádi and Nemeskéri 1970; Ferembach *et al.* 1979; Sjøvold 1988; Buikstra and Ubelaker 1994). For the children, determining criteria were noted when present, but only in some cases estimates were made because of the mainly very young age of most infants combined with the poor preservation of the skeletons.

The following age groups were used (Buikstra and Ubelaker 1994): Infants Ia (0-3 years), Infants Ib (3-6 years); Children (6-12 years). Age determination in infants and children was conducted using the dental development (Ubelaker 1978) as well as the long bone length (Fazekas and Kósa 1978; Scheuer and Black 2000), sizes of the pelvis and scapula (Florkowski and Kozłowski 1994) and the state of fusion of the bodies and arches of the vertebrae (Schwörer 1975). Age determination in adults was based on the degree of dental wear (Brothwell 1981; Perizonius and Pot 1981), the state of fusion of the cranial sutures (Vallois 1937), as well as the presence and severity of degenerative joint changes and osteoporosis.

Non-metric traits were scored systematically for the teeth (Alt 1997; Edgar 2017) and non-systematically for the cranium and postcranium (Hauser and DeStefano 1989; Mann *et al.* 2016). On the cranium, the presence and number of Wormian bones, *sutura* mendosa and *metopica*, on the postcranium the presence of the *foramen supratrochleare* on the distal humerus was noted.

Pathological changes of the teeth were recorded by the methods of Schultz (1988) for the degree of calculus and the expression of linear enamel hypoplasia. Dental wear was recorded using the method of Perizonius and Pot (1981) and Brothwell (1981); numbering of teeth after Fédération Dentaire Internationale (FDI).

In 27 individuals aDNA samples were taken to test for a genetic relationship, but the collagen content of the samples (petrous bones and teeth) was not sufficient to provide valid results. Only in three individuals, results could be achieved (Skourtanioti and Feldman this volume).

Results

Representation, Preservation, and Surface Composition

Representation varies considerably among the skeletons, ranging from 5% of the whole skeleton preserved (1% for the additional bones Loc. CR6:41a-c in the Burial CG6, Loc. CR6:40) to 100% preservation. The representation seems to be better in the younger age groups (Table 2), but also one of the older infants and a child are well represented. There is no significant difference in representation between skeletons of single or double burials. However, in the multiple burial of four infants in Burial CG9, Loc. CR28.2:122a-b/123a-b, representation is lowest, ranging between 5-35%. Representation of skeletons also does not differ between the various rooms.

Preservation is best in the bones of the youngest individuals (Table 2). A solid bone structure is present in one of the youngest infants, while all other individuals in the younger age group exhibit a fragile bone structure. In contrast, the older age groups mainly show a very fragile bone structure. Surface compositions seem to follow a similar trend (Table 2), with less erosion observed on the surface of the bones from younger individuals. However, the distribution of surface preservation is less clear compared to the preservation of the bones.

Fig. 9 Posterior view of the left femur of CG10, Loc. C10:408.8 with gnawing marks of rodents. (Photo: J. Gresky, Ba`ja N.P., DAI)

Fig. 10 Anterior view of the left femur of the adult male in CG10, Loc. C10:408.8 with severe plant root etching, the roots still being in place. (Photo: J. Gresky, Ba`ja N.P., DAI)

Table 3 All skeletons and additional bones and their affecting taphonomic agents: black and red staining, presence of crystals, rodent gnawing marks, and plant root etching. To facilitate a better comparison of the factors to age groups, the latter were combined into five classes: around birth, younger and older infants, child, and adult.

Room	Locus	Age	Black Staining			Red Staining		Crystals	Rodent Gnawing Marks	Plant Roots
			few black spots	many black spots	other colouration	red spots	red all over			
CR35	C10:408.8	adult		1					1	1
CR35	C10:405-I	around birth	1							
CR35	C10:405-II	older infant	1							
CR36.1	C1:46	child	1				1			
CR6	CR6:23a	older infant		1	dark stripes right parietal	1				
CR6	CR6:23b	younger infant			dark external, lighter internal surface					
CR6	CR6:40	around birth		1						
CR6	CR6:41a	adult		1				1	1	
CR6	CR6:41b and c	around birth		1						
CR6	CR6:48	child		1						
DR19	DR19:110	around birth	1							1
CR5	CR5:49A	younger infant	1							
CR5	CR5:54	younger infant	1			1				
CR5	CR5:53	older infant		1						1
CR28.2	CR28.2:122a	older infant		1						
CR28.2	CR28.2:122b	older infant		1						
CR28.2	CR28.2:123a	around birth		1						
CR28.2	CR28.2:123b	around birth		1						

Black and Red Staining, Presence of Crystals, Rodent Gnawing Marks, and Plant Root Etching

Black staining can be observed as either a few or many black spots (Table 3). These spots are present in all individuals except for the younger infant of Burial CG5, Loc. CR6:23b, whose bones have a continuous dark external surface and a lighter internal surface. Among the individuals, six display a few dark spots, while eleven have many distributed throughout their skeletons. There does not seem to be any relation to the age group. Skeletons of double burials mainly have similar amounts of dark spots, except for the two in Burial CG2, Loci CR5:53 and CR5:54. Red staining only occurs in three individuals: the younger infant of Burial CG2, Loc. CR5:54 has some red spots on the right frontal (Fig. 7), whereas the older infant of Burial CG5, Loc. CR6:23a (Fig. 4) has an intentional spot-like colouration, and the child of Burial CG7, Loc. C1:46, is covered by red staining (Figs. 5-6). Crystals could only be detected in the additional adult lower arm bones in Burial CG6, Loc. CR6:41a (Haddow this volume). Gnawing marks from rodents are only present on adult bones: particularly severe on the single inhumation of Burial CG10, Loc. C10:408.8 (Fig. 10), and on one of the additional adult bones of Burial CG6, Loc. CR6:41a. Plant root etching was observed in three individuals: Burial CG10, Loc. C10:408.8 (Fig. 9), in the older infant of Burial CG2, Loc. CR5:53 (Fig. 8), and a very young infant in Burial DG2, Loc. DR19:110.

Age and Sex Profile

The determination of sex was mostly impossible due to the poor preservation of the skeletons and their young age. The only adult was determined to be male rather than female. Out of 15 infants and children, in 11 cases, no sex determination was possible. In the three oldest children (4-8 years) a female rather than male sex was suggested, primarily based on characteristics of the mandible. In one of the infants (Burial CG8, Loc. C10:405-I), a female sex was genetically determined (Feldman *et al.* 2019), although the morphological characteristics of the mandible suggested a rather male sex for the child.

Age estimation: One young adult was determined to be between 25-35 years of age.

Of the 15 other individuals, five died at a very young age between 9.5 lunar months and 6-9 months. Five died between 3-4 years. Three individuals reached the age between 1.5 and 3 years and two died between 7 to 8 years of age. The two oldest were buried in single burials, however two of the youngest age group (0 years) and 0 years (± 2 months) as well as

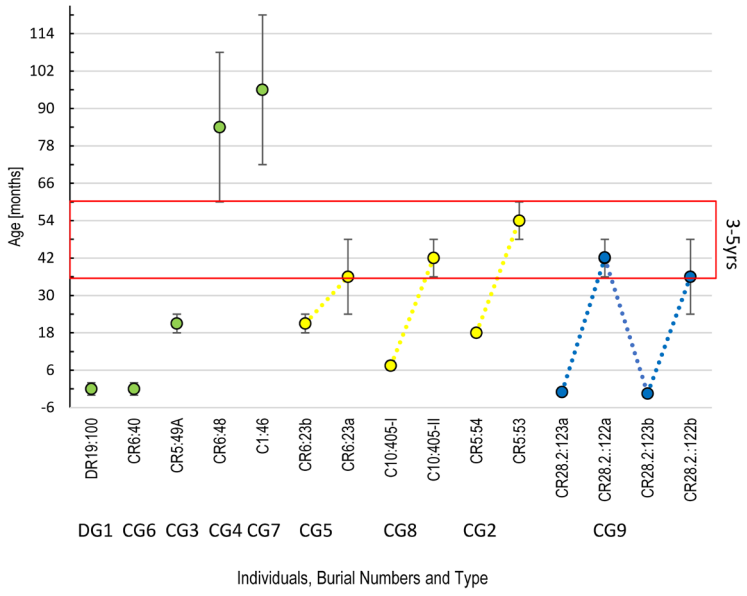

Fig. 11 Individuals sorted by age class and burial type. Single burials marked in green, double burials in yellow, and the multiple burial in blue. (Graph: M. Benz, Ba`ja N.P.)

one 1.5-2 year-old individual were buried in single burials, all in different rooms, CR5, CR6, und DR19. The three double burials, located in three different rooms, CR5, CR6, and CR35, each include a 3-4 year-old child accompanied by a younger one: one is 6-9 months, two are 1.5-2 years old. The only multiple burial CG9 in Room CR28.2 consists of two 3 year-old individuals buried together with two 9.5-10 lunar-month-old individuals (Fig. 11).

Non-Metric Traits

Non-metric traits on the skull were visible on two individuals: one child from the single Burial CG4, Loc. CR6:48, being 7 years (± 24 months) of age and one older infant from the double Burial CG2, Loc. CR5:53, being 4 years (+ 12 months) of age. Both showed Wormian bones, extra small bones that can occur within a suture of the skull. The younger child had up to eleven Wormian bones in the posterior sagittal suture and lambda suture (Figs. 12, S53-1, S53-2).[1] Both showed a *sutura* mendosa (Fig. S53-3, arrow), the older one also a remnant of the *sutura metopica*.

In the postcranium, the older one (CG4, Loc. CR6:48) had a *foramen supratrochleare* on both humeri (Fig. S48-10).

Dental traits like shoveling (Figs. 13, S53-9) and Carabelli's cusp (Fig. 14) occurred more frequently in several individuals, and will be published separately. There is no evidence of congenital absence of teeth.

[1] All figure numbers beginning with 'S' and including the Individual ID-Number refer to the catalogue entry of the specific individual, where all figures related to that individual are compiled.

Fig. 12 Dorsal view of the occipital and both parietal bones of CG2, Loc. CR5:53 with at least 11 Wormian bones (indicated by numbers) as well as two additional small sutures (marked red). (Photo: J. Gresky, Ba`ja N.P., DAI)

Fig. 13 Shoveling of the lingual surface of tooth 12 of CG2, Loc. CR5:53. (Photo: J. Gresky, Ba`ja N.P., DAI)

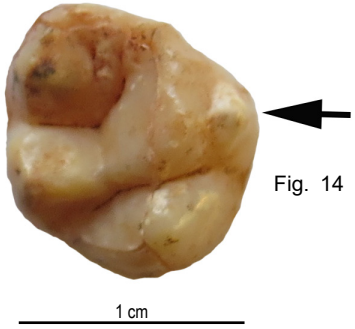

Fig. 14 Carabelli´s cusp (arrow) on the lingual surface of tooth 16 of CG7, Loc. C1:46. (Photo: J. Gresky, Ba`ja N.P., DAI)

Table 4 Pathological changes of the cranium. If not divided in left and right, the diagnosis in orbital roofs includes both sites.

Room	Locus	Age	*Lamina Externa*	*Lamina Interna*	Orbital Roof
CR35	C10:408.8	adult	not preserved	not preserved	not preserved
CR35	C10:405-I	around birth	porous lambda	porous new bone formations	porous
CR35	C10:405-II	older infant	porous lambda	whitish porous plates, small roundish pit-like impressions	porous
CR36.1	C1:46	child	not preserved	not preserved	not preserved
CR6	CR6:23a	older infant	healthy	porous bone formation	not preserved
CR6	CR6:23b	younger infant	not preserved	not preserved	not preserved
CR6	CR6:40	around birth	healthy	lingulate, plaque-like new bone formations	flaky
CR6	CR6:48	child	healthy	whitish porous plates, small roundish pit-like impressions	healthy
DR19	DR19:110	around birth	porous (growth)	lingulate, plaque-like new bone	healthy
CR5	CR5:49A	younger infant	not preserved	not preserved	not preserved
CR5	CR5:54	younger infant	porous	whitish porous bone formations	right healthy, left not preserved
CR5	CR5:53	older infant	porous	whitish porous bone formations cranial base	right porous, left not preserved
CR28.2	CR28.2:122a	older infant	not preserved	not preserved	not preserved
CR28.2	CR28.2:122b	older infant	not preserved	not preserved	not preserved
CR28.2	CR28.2:123a	around birth	not preserved	not preserved	not preserved
CR28.2	CR28.2:123b	around birth	not preserved	not preserved	not preserved

Fig. 15 Internal lamina of the occipital bone of CG8, Loc. C10:405-I showing new bone formations, mainly loosely connected to the surface but also more densely attached to it. (Photo: J. Gresky, Ba`ja N.P., DAI)

Pathological Changes

Cranium: Due to the poor preservation, pathological changes of the bones were only visible in some of the individuals (Table 4). In the only adult, the preservation of the cranial bones was so poor that no further changes could be observed. The same applies to most of the non-adult cranial bones. Therefore, the changes are described only when present, but no frequencies can be estimated. The generally very young age of the individuals limited the number of affected areas, *e.g.*, in most cases, paranasal sinuses had not yet developed.

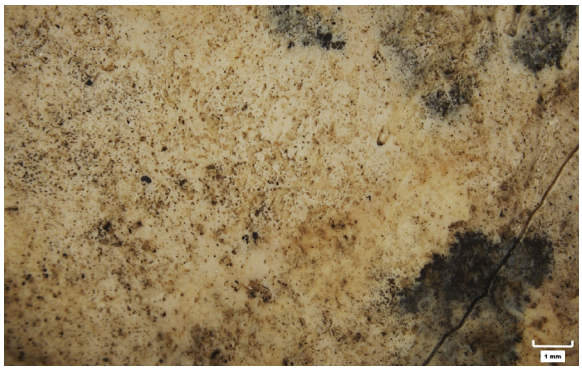

Fig. 16 Detail of the internal lamina of the right frontal bone close to the coronal suture of CG2, Loc. CR5:54 with new bone formations loosely connected to the surface. (Photo: J. Dorn, DAI)

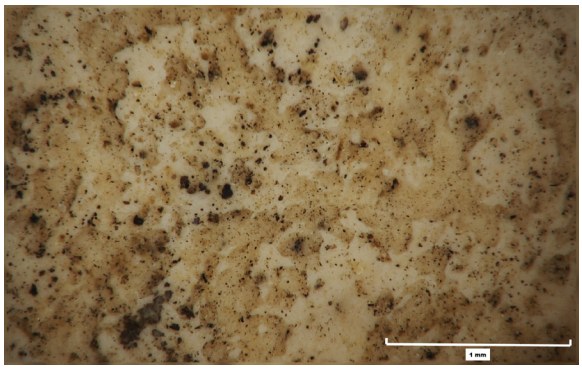

Fig. 17 Detail of Fig. 16 with small whitish plate like bone formation. (Photo: J. Dorn, DAI)

Fig. 18 Detail of the internal lamina of the right squama temporalis of CG2, Loc. CR5:53 with new bone formations more densely connected to the surface. (Photo: J. Dorn, DAI)

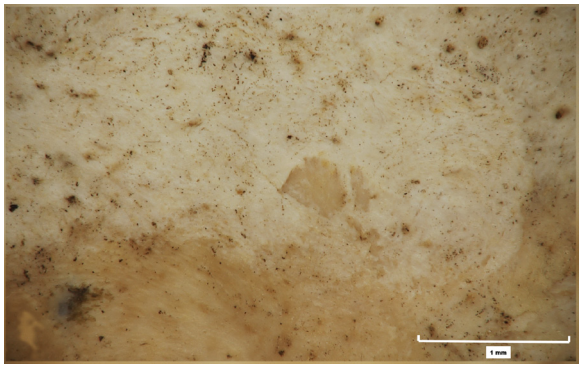

Fig. 19 Detail of Fig. 18 of the transition of the whitish plate-like bone formation to the original bone. (Photo: J. Dorn, DAI)

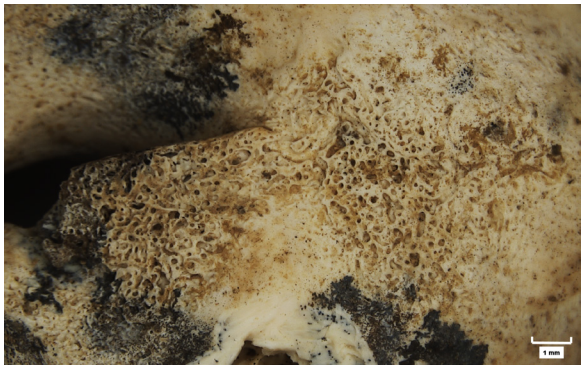

Fig. 20 Detail of the right ala major of CG4, Loc. CR6:48 with thick layers of newly formed bone. (Photo: J. Dorn, DAI)

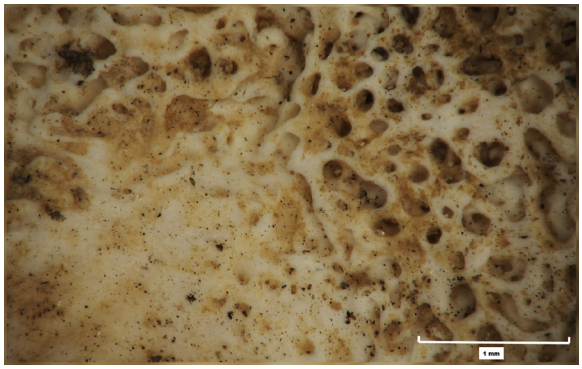

Fig. 21 Detail of Fig. 20 of the transition of the thick plate-like bone formation to the original bone. (Photo: J. Dorn, DAI)

Lamina externa: Pathological changes of the external lamina of the cranial bones were observed in five out of eight individuals with preserved cranial vault. In four individuals (both individuals of the double Burials CG8, Loci C10:405-I and C10:405-II, and CG2, Loci CR5:53 and CR5:54), there was a noticeable porosity in the parietal bones close to the lambda suture (Figs. S53-2, S54-1, S405.I-1, S405.II-1). In one individual (DG2, Loc. DR19:110), the general porosity seems to be related to physiological growth. However, on the occipital bone, there is a 6 x 6mm widened area with slight porous surface and an impression of blood vessel running through the area (Figs. S110-1, S110-2).

Table 5 Pathological dental features of all individuals with preserved teeth. LM=lunar month, mths=months, yrs=years.

Room	Locus	Age	Calculus	Dental Wear Permanenty	Dental Wear Deciduous	Chipping	Hypoplasia	Age of Hypoplasia (yrs)
CR35	C10:408.8	25-35 yrs	in all teeth grade I-II	anterior (grade 4-5), posterior left (grade 2-5) right (grade 2-3)		10/18 teeth, mainly posterior dentition and singular <1-4x4mm	transverse	5,6,7,12
CR35	C10:405-I	6-9 mths	no		0	none	spot	7 ± 2 mths. in utero
CR35	C10:405-II	3-4 yrs	two teeth with grade I		anterior (grade 2-3) posterior (grade 1-2)	small on tooth 84	transverse, spot, roots	2
CR36.1	C1:46	8 yrs (± 24 mths)	lower incisivi grade I	grade 1-2	anterior and posterior (grade 3-4)	none	transverse, spot	4,5,6,7
CR6	CR6:23a	3 yrs (± 12 mths)	no		anterior (grade 1-2+) posterior (grade 1).	none	transverse	3
CR6	CR6:40	0 yrs (± 2 mths)	no		0	none	none	
CR6	CR6:48	7 yrs (± 24 mths)	lower incisivi grade I-II	grade 1-2	anterior and posterior (grade 4-5)	multiple small on teeth 53, 61, 63, 64, 75, 84, a deeper one on 63	transverse, spot, roots	3,4,5,6,7
DR19	DR19:110	0 yrs	no		0	none	none	
CR5	CR5:53	4 yrs (+ 12 mths)	upper premolars grade I-II		anterior (grade 4-4+) posterior (grade [3] 4-5)	none	transverse, spot, roots	1,3,4
CR5	CR5:54	1.5 yrs	lower incisivus grade I		anterior (grade 2)	none	none	
CR28.2	CR28.2:122a	3 yrs (+ 12 mths)	no		0	none	none	
CR28.2	CR28.2:122b	3 yrs (± 12 mths)	no		0	none	none	
CR28.2	CR28.2:123a	9.5 LM	no		0	none	none	

Lamina interna: The internal lamina of the cranial bones showed pathological changes in all eight individuals with preserved cranial vault and base. The changes manifested as porous new bone formations attached to the internal lamina. Some of these new bone formations appeared more 'unorganised' and loosely connected to the surface, while others were already more densely attached to the internal lamina (Fig. 15). Lingulate new bone formations were observed in two individuals of 0 years (± 2 months) of age in the frontal and parietal *tubera* region (CG6, Loc. CR6:40; DG2, Loc. DR19:110) (Figs. S40-1, S110-3). These formations are likely associated with the physiological growth process. A mixture of less (Figs. 16-17) and more (Figs. 18-19) remodeled new bone formation can be found in four individuals of different ages (Loci C10:405-I, CR6:23a, CR6:48, CR5:54). The bone formations are mainly located on the caudal base of the frontal bone, the occipital as well as in the impressions of the cranial base (Figs. 20-21, S405.I-2 to S405.I-4, S23a-1, S48-3, S54-2, S54-3). In two of the older individuals (Loci CR5:53; C10:405-II) remodeled bone formations only occur again at the base of the frontal and occipital bone and in the *impressiones digitatae* of the temporal bone (Figs. 18-19, S53-4, S405.II-4).

Fig. 22 Labial surface of tooth 42 of CG4, Loc. CR6:48 with remnants of calculus (grade I). (Photo: J. Gresky, Ba`ja N.P., DAI)

Fig. 23 Labial surface of tooth 61 of CG2, Loc. CR5:54 with remnants of calculus (grade I). (Photo: J. Gresky, Ba`ja N.P., DAI)

Fig. 24 View of the occlusal surface of the mandibular teeth of CG2, Loc. CR5:53 with exceptional wear relative to the age of 4 years (+12 months). (Photo: J. Gresky, Ba`ja N.P., DAI)

Additionally, two older individuals (Loci CR6:48, CR35:405-II) showed small roundish pit-like impressions (Fig. S48-2) on the lateral aspects of the base of the frontal bones and anterior cranial fossa. Two of the older individuals (Loci C10:405-II; CR6:23a) exhibited new bone formation within the impressions of the *sagittal*, transverse, and sigmoid sulci.

Orbital roofs: Porosity of the orbital roof was present in three out of seven individuals. As fine porous surface covering both orbitae in individual Loc. C10:405-I (Fig. S405.I-5), and as less severe, more coarse porosity in both orbital roofs of individual Loc. C10:405-II (Fig. S405.II-5). The right orbital roof of individual Loc. CR5:53 shows a small blood vessel impression, which is surrounded by a fine porous 5 x 2mm area (Figs. S53-5, S53-6).

Teeth: Due to the poor preservation and limited number of present teeth, pathological features of teeth are described by individual (Table 5). No cases of caries and periapical processes were recorded in any of the individuals.

Calculus: In the adult individual (Loc. C10: 408.8), calculus is present on all of the teeth to a low to moderate degree (grade I-II, after Schultz 1988; Fig. S408.8-2). In the other individuals, particularly the children (Loci C1:46; CR6:48, Fig. 22), calculus was observed in low degrees (grade I-II), but also the younger ones, the 3-4 year-old (Loci C10:405-II; CR5:53, Fig. S53-7) and already one of the 1.5 year-old individual (Loc. CR5:54, Fig. 23) were affected.

Dental wear: In the adult individual (Loc. C10:408.8), dental wear is severe in the anterior dentition (grade 4-5) (Fig. S408.8-1), while it differs in the posterior dentition between the left (grade 2-5) and right side (grade 2-3). In the two children aged 7 and 8 years (Loci CR1:46; CR6:48), the anterior and posterior permanent dentition shows only slight wear (grade 1-2). However, the wear of the deciduous teeth exhibited higher degrees, between grade 4-5 in the 7 year-old (± 24 months) individual and between grade 3-4 in the 8 year-old (± 24 months) individual (Fig. S48-4). The deciduous dentition of the youngest individuals, ranging between 1.5 and 3-4 years of age (Loci CR5:54; C10:405-II; CR6:23a), shows low degrees of wear between grade 1-2, with the anterior dentition slightly more worn than the posterior. An exceptional wear relative to age is visible in both the anterior dentition (grade 4-4+) and posterior dentition (grade [3] 4-5) of the 4 year-old (+ 12 months) individual (Loc. CR5:53) (Fig. 24).

Chipping: Chipping of small flakes of enamel is only present in three individuals: The adult individual (Loc. C10:408.8) shows enamel chipping on 10/18 teeth, mainly in the posterior

dentition. Chippings occur mainly singular, ranging from less than 1mm to 4 x 4mm in size (see catalogue: Fig. S408.8-2). The 7 year-old (± 24 months) individual (Loc. CR6:48) shows multiple small chippings of enamel on several teeth (tooth numbers: 53, 61, 63, 64, 75, 84) and a deeper one on the upper left canine (63). The 3-4 year-old individual (Loc. C10:405-II) has a small enamel chipping on the distal occlusal surface of the first right molar of the mandible (84).

Linear enamel hypoplasia: In the adult individual (Loc. C10:408.8), linear enamel hypoplasia was observed on 11/18 teeth, with a moderate expression (grade II, Schultz 1988; see catalogue: Fig. S408.8-1). Their occurrence can be related to ages between 5 to 7 and 12 years (Ubelaker 1978).

Of 12 non-adults with preserved teeth, six showed enamel hypoplasia, mainly linear, but sometimes also spot-like.

The 8 year-old (± 24 months) individual (Loc. C1:46) has transverse linear enamel hypoplasia on several teeth (grade I: 11, 31-32, 42; grade II: 13, 17, 23, 43). Their occurrence can be related to ages between 4 to 7 years.

The 7 year-old (± 24 months) individual (Loc. CR6:48) shows transverse linear enamel hypoplasia on many teeth (grade I: 14-15, 24-25, 31, 37, 41; grade II: 12-13, 22-23, 32-35 [Fig. S48-5], 42-45). Their occurrence can be related to ages between 3 to 7 years. Additionally, a spot-like enamel hypoplasia was present on the right first premolar of the mandible (44), its age of occurrence is at *c*. 3 years. Transverse lines were visible on the roots of the left and right first molar of the mandible (36, 46; Fig. S48-6).

The 4 year-old (+ 12 months) individual (Loc. CR5:53) has transverse linear enamel hypoplasia on many teeth (grade I: 15-16, 25; grade II: 11-14, 21-24, 33-34, Fig. S53-8). Their occurrence can be related to ages between 3 to 4 years. Additionally, a spot-like enamel hypoplasia was present on the upper right central incisor (11), which occurred at an age of *c*. 1 year.

The 3-4 year-old individual Loc. C10:405-II has transverse linear enamel hypoplasia on four teeth (grade I: 16, 26 41, 42), indicating an age of occurrence of *c*. 2 years. A spot-like enamel hypoplasia is on the lower right central incisor (41).

The 3 year-old (± 12 months) individual, Loc. CR6:23a, shows transverse linear enamel hypoplasia on seven teeth of the permanent dentition (grade I: 11, 21, 31-32, 41; grade II: 16, 26), indicating an age of occurrence of *c*. 3 years.

The 6-9 month-old female, Loc. C10:405-I, shows spot-like enamel hypoplasia on her lower right central incisor (81), which occurred at an age of *c*. 7 ± 2 months in utero.

Enamel hypoplasia most often occurs between the ages of 3-7 years (Fig. 25). It is important to note that the young age of the individuals limits observations for ages older than 4-5 years.

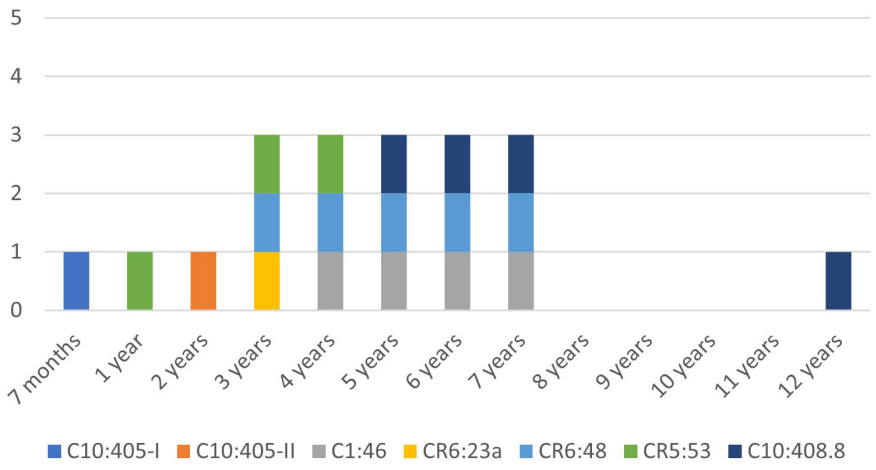

Fig. 25 Transverse and enamel hypoplasia and their approximate time of development. The y-axis shows the number of individuals exhibiting enamel hypoplasia. (Graph: J. Gresky, Ba`ja N.P., DAI)

However, in the younger age groups, the development of hypoplasia is relatively infrequent.

Interproximal grooving: Interproximal grooving can be evidenced in the adult individual Loc. C10:408.8 in the first and second molars of the left maxilla (26, 27; see catalogue: Figs. S408.8-3 to S408.8-5). The straight shallow grooves with a semicircular diameter are visible on the mesial surface (7 x 1mm) of tooth 26 and on its distal surface (5 x 1.2mm), which opposites the shallow groove on the lingual half of the mesial surface (4 x 1mm) of tooth 27. The neighbouring tooth 25 shows no groove. The molars (18, 28, 36) also do not show interproximal grooving, while all the other molars are too poorly preserved, and the area of interest is mainly missing.

Postcranium (Table 6): Possible well-healed traumatic changes can be observed in the distal phalanx of the first left toe of individual Loc. CR5:53 (4 years + 12 months). The distal joint surface is slightly depressed showing a v-shaped fissure (Figs. S53-14 to S53-16). Another possibly healed fracture is visible in the middle phalanx of the second right finger of individual Loc. CR6:48 (7 years ± 24 months). This fracture manifests as flattening of the distal half, with slight enlargement of the ulnar condyle and small foramina arranged in a row on the dorsal surface (Figs. S48-12, S48-13). In two children and one infant, ribs showed changes: one case (Loc. CR6:23a) was identified as definitely traumatic, while the other two cases (Loci CR6:48; CR5:49A) were possibly due to anatomic variation. In Loc. CR6:23a (3 years ± 12 months), a pseudarthrosis developed following a fracture of two middle (between 7-9) right ribs, located directly sternal to the rib neck joint (Figs. S23a-2 to S23a-8). The right 8th-11th ribs of Loc. CR6:48 (7 years ± 24 months) have an

Table 6 Pathological features and variations of the postcranium.

Room	Locus	Age	Sex	Trunk	Extremities
CR35	C10:408.8	adult	m>=f	healthy	healthy
CR35	C10:405-I	around birth	f	healthy	healthy
CR35	C10:405-II	older infant	m=f	healthy	bowing of the right femur, flattened proximal quarter of both humeri
CR36.1	C1:46	child	f	healthy	pronounced attachments of M. soleus, M. deltoideus
CR6	CR6:23a	older infant	m=f	two right middle ribs (7-9): pseudarthrosis sternal of the rib neck joint	healthy
CR6	CR6:23b	younger infant	m=f	healthy	healthy
CR6	CR6:40	around birth	m=f	flaring of sternal ends of ribs	flaring ends of long bones
CR6	CR6:48	child	f>=m	right 8th-11th ribs in the region of the angulus have an extension to the inferior rim	healed fracture? middle phalanx of the second right finger, cribrosity both femoral necks, Harris lines tibia and femur
DR19	DR19:110	around birth	m=f	healthy	enlargement of proximal ends of humerus, femur and tibia
CR5	CR5:49A	younger infant	m=f	10th right rib has two notches of the inferior rim	healthy
CR5	CR5:54	younger infant	m=f	not present	decrease in width in comparison to length of all long bones
CR5	CR5:53	older infant	f>m	healthy	fracture? distal phalanx of the first left toe
CR28.2	CR28.2:122a	older infant	m=f	not present	healthy
CR28.2	CR28.2:122b	older infant	m=f	not present	healthy
CR28.2	CR28.2:123a	around birth	m=f	not present	healthy
CR28.2	CR28.2:123b	around birth	m=f	not present	healthy

extension of the inferior rims in the region of the *angulus* (Figs. S48-7 to S48-9). In the infant, Loc. CR5:49A (1.5-2 years), two notches are present on the inferior rim of the 10th right rib (Fig. S49A-1, S49A-2).

Loc. C1:46 (8 years ± 24 months) shows pronounced attachments of the *musculus soleus* and *musculus deltoideus*.

On both anterior femoral necks, a cribrosity is visible in individual Loc. CR6:48 (7 years ± 24 months) (Fig. S48-14). Harris lines can be observed in the postmortem broken ends in the right distal femur and both distal tibiae (Fig. S48-15). The radiographs show multiple Harris lines in the distal and most of the proximal ends of all long bones (Figs. S48-16, S48-17).

In individual Loc. DR19:110 (0 years), an enlargement, more specifically flaring of the proximal ends of humerus, femur, and tibia is evident (Figs. S110-4 to S110-11). Similarly, in individual Loc. CR6:40 (0 years ± 2 months), there is a flaring of the ends of long bones (Fig. S40-3) and sternal ends of ribs (Fig. S40-2).

The child Loc. C10:405-II (3-4 years) shows severe bowing of the shaft of the right femur to ventral but without deformation (Fig. S405.II-7) and a flattened proximal quarter of both humeri (Fig. S405.II-6).

In individual Loc. CR5:53, all long bones show a reduced width compared to their length giving them a very gracile appearance (Figs. S53-10 to S53-13).

Discussion

To contextualise the results obtained from the skeletons in Ba`ja, comparisons with individuals from other Neolithic Jordanian sites, such as Shkārat Msaied (Hermansen *et al.* 2006; Kinzel *et al.* 2017), ‘Ain Ghazal (Rollefson *et al.* 1985), and Basta (Schultz *et al.* 2004, 2007) were conducted, although these studies mainly include adult individuals. The Neolithic site of Shir in Syria was utilised as a reference (Gresky *et al*. 2018) for a direct comparison with a larger group of non-adults.

Shkārat Msaied is a Neolithic site in Southern Jordan, 13km north of Petra in a semi-arid sandstone mountain area. The settlement of circular-shaped permanent stone buildings dates to 8340-7900 cal BCE. The inhabitants were supposed to have a relative mobile or semi-sedentary life style. So far, a minimum of 32 individuals (two infants/ newborn, three non-adults) were found in primary and secondary burials, tertiary deposits and disarticulated and fragmented human remains in the fill. There are no pathological changes described in the individuals so far (Hermansen *et al.* 2006; Kinzel *et al.* 2017).

‘Ain Ghazal is one of the largest so-called mega-sites of the early Neolithic. It is located at the River Nahr ez-Zarqa in the Jordanian capital of Amman. Its Pre-Pottery Neolithic B/C (PPNB/C) occupation dates between *c*. 8400-6600 cal BCE. 80 individuals have been found (24 infants, 14 children, 4 adolescents, 38 adults) (Rollefson *et al.* 1985; Grindell 1998).

Basta is a Late PPNB settlement about 20km to the southeast of Ba`ja, dating to 7540-7040 cal BCE. It is located near a permanent spring but also close to dry-steppe environments (Nissen *et al*. 2004; Gebel *et al*. 2006). Within the large settlement below the floors primary and secondary burials have been found as well as five skull deposits and numerous isolated human bones. For osteological analyses 39 individuals were present, 19 adults and 20 non-adults (3 fetuses, 17 infants, and children) (Schultz *et al.* 2004, 2007).

Shir is a Neolithic settlement site near the modern town of Hama in Western Syria dating to 7000-6450/6400 cal BCE. It is located in close vicinity to the Orontes River and is situated in a fertile landscape (Bartl 2018). The mainly single burials were either placed in the buildings or had some association to them (Resch and Gresky 2018). 51 burials and bone depositions were found comprising altogether 77 individuals but spanning different chronological layers. 65 individuals were younger than 12 years (84.4%), of which 57 were infants, five children, three of unknown age. Only five adolescents and seven adults were in the sample (Gresky *et al.* 2018).

Taphonomy

In general, preservation of bone in Neolithic burials in Jordan is known to be quite poor due to climatic conditions and soil composition. Consequently, invasive methods such as isotopic and genetic analyses cannot be adequately applied due to the insufficient preservation of

bone collagen. In the case of Ba`ja, C/N-isotopic analyses failed (see Benz *et al.* this volume Part 2: Appendix 4), and only three out of 27 samples yielded valid results for genetic investigations because of the poor preservation of collagen (Skourtanioti and Feldman this volume). While in Shkārat Msaied the bones of the described two infant skeletons were very brittle (Kinzel *et al.* 2017), the preservation of bones in Basta was mainly very good (Schultz *et al.* 2007). However, it should be noted that mostly the fetuses and neonates were less well preserved. This contrasts with Ba`ja, where preservation of the younger individuals is better than that of older individuals.

Within the single burials in Ba`ja, a sufficient representation is strongly connected to the good preservation of the bones. Interestingly, the representation and preservation do not differ significantly between individuals in single or double burials. One would expect that single burials would represent primary, not further disturbed burials and therefore show a better bone preservation. The three double burials show different patterns in preservation of the two individuals. This observation suggests possible differences in burial practices. However in the double Burial CG8, Loci C10:405-I-II, the representation and preservation of the bones in both individuals are similar, indicating a simultaneous deposition of the bodies. This interpretation is further supported by the very close positioning of the individuals. In contrast, in the double Burial CG5, Loci CR6:23a-b, there is a significant difference in the representation and preservation of the two individuals, although they should have been buried together in one event because the younger individual, Loc. CR6:23b, laid between the upper and lower halves of the body of individual Loc. CR6:23a. In the double Burial CG2, Loci CR5:53-54, the representation of the two individuals differs a lot. It seems like the younger individual has been placed into the grave first and was later disturbed by putting individual Loc. CR5-54 into the same grave. This theory would be supported by the difference in black staining (Table 3). However, a simultaneous deposition cannot be excluded.

The four infant skeletons of the multiple burial CG9, Loci CR28.2:122a-b/123a-b, show a very poor preservation of bones and representation of the skeletons. There are no significant differences between them, although the oldest one is the least represented. This might indicate that they were buried together and were influenced by the same environment over a long period leading to equal destruction of the bones of all skeletons.

Judging by the representation, it appears that the whole body was buried in most of the individuals. Only individual Loc. CR6:23b is missing the bones of the skull, except for the *clivus*. This could potentially be attributed to the poor preservation, which may account for most of the missing parts. In the case of individual Loc. CR5:49A, the skull is missing, but the first cervical vertebra was present. It is possible that the skull was already damaged because the grave was not covered by stones. A skeleton in this position was not to be expected so it might have been destroyed until the grave became visible. A similar case is reported from Shkārat Msaied (Kinzel *et al.* 2017), where a 0-1 month-old individual is missing the skull, and intentional removal is discussed as a possibility.

Additional isolated bone elements have been found in Loci CR6:41a of at least two adults, CR6:41b of an infant around birth, and a fetus (CR6:41c). These do not represent burials but clearly single bones or elements which might have been either remnants from earlier burials or were placed there deliberately. Single bone elements are also known from Basta and Shkārat Msaied (Schultz *et al.* 2007; Kinzel *et al.* 2017) and are discussed as remnants of disturbed burials.

Black staining is discussed as being due to manganese in the surrounding soil (*e.g.*, López-González *et al.* 2006). Skeletons in double burials generally show the same amount of dark spots, except for the two in Burial CG2, Loci CR5:53 and CR5:54, which may indicate a potential difference in burial treatment. Red staining of bones (Gebel b this volume) seems to be due to human impact at least in one individual: child Loc. C1:46 is covered by red staining (Benz *et al.* 2020, this volume, Part 2). The two other individuals, Loc. CR6:23a with an intentional spot like colouration and Loc. CR5:54 with some red spots on the right frontal bone, could potentially be deliberately stained. However, it is also possible that they acquired the spot-like colouration by red pigments in the surrounding soil (Reifarth *et al.* this volume). Colouring with red pigments is already known from Natufian burial sites, *e.g.*, Shubayqa 1 in northeast Jordan (Richter *et al.* 2019), where four perinates and infants showed evidence of treatment with ochre.

Crystals were only detected in the additional adult lower arm bones of Loc. CR6:41a (Haddow this volume). This observation might indicate that these bones had been buried somewhere else before being placed in the grave of the infant.

Rodent gnawing marks were restricted to adult bones. Severe gnawing marks were evident on the bones of the single inhumation Loc. C10:408.8, and on one of the additional adult bones Loc. CR6:41a. Rodent gnawing marks typically occur when bones are devoid of soft tissue, and rodents utilise the calcium for consumption and to abrade their teeth. The preference for adult bones over non-adult bones may have practical reasons, as the non-adult bones may be too small for the purpose of abrasion.

Age and Sex Profile

The very poor preservation and the presence of mainly infants and children in the sample prohibited a sex determination in most of the individuals. Within these limits, anthropological and genetic analyses determined male and female sexes of the individuals (Feldman *et al.* 2019; Skourtanioti and Feldman this volume). Although all four individuals for whom sex could be determined showed a female sex (one genetically and three anthropologically), no conclusion can be drawn regarding a sex predilection.

Except for one young adult male from a single burial, within the single or double burials, so far, only non-adult individuals could be found. This is in contrast to the collective burials also present at the site that contain individuals of all age categories (in preparation). Single or double burials of infants and children under the floor of rooms match the burial patterns in many other PPN sites, where adults are less often buried in the area of the houses.

In Ba`ja, the largest number, 13 out of 15 non-adults, died at a very young age (between 9.5 lunar months and 6-9 months and between 3-4 years of age). Only two died at an older age, between seven to eight years. In Basta, 57% (n=32/56) of the individuals were non-adults; fetuses and neonates account for 10.7% (n=6) (Schultz *et al.* 2007). In 'Ain Ghazal, 47.5% (n=24 infants + 14 children/ 80 individuals) of the individuals were non-adults, and infant mortality within the first year of life was high (Rollefson *et al.* 1985), discussed by the authors as a particularly dangerous period in the Neolithic village. In Shir, the majority of individuals died before reaching 12 years of age (84.4%, n=65/ 77). When including the five adolescents, this proportion increases to 90.9% (Gresky *et al.* 2018). Here too, most of the individuals (n=54) died within the first year of life. In all sites, but particularly at the site of Shir, the high number of non-adults is strongly influenced by burial customs, as adults were not buried within the settlement area.

The high number of deaths in the first year of life can be explained by the vulnerability of newborns who have a less developed immune system. This pattern is commonly observed in populations with low life expectancy (Drenhaus 1992).

Interestingly, the five individuals who died between the ages of 3-4 years were all buried together with one individual of the youngest age group. It remains uncertain whether these pairs are siblings or just died at the same time and were consequently buried together. This phenomenon is not known from other PPN sites from the Levant so far.

The choice of a single or double burial does not seem to be related to the age of infants and children: The two oldest individuals were buried in single burials, but also two of the youngest individuals of the age group (0 years and 0 years ± 2 months) as well as one 1.5-2 year-old individual were found in single burials.

Non-Metric Traits

Non-metric traits are heritable alterations that are not caused by sequence changes in the DNA but by modification of gene expressions (*e.g.,* Dupont *et al.* 2009). They tend to cluster in individuals who are closely related genetically (Alt 1997; Alt *et al.* 2013; Edgar 2017). Unfortunately, due to the poor preservation, only a few non-metric traits could be documented. Only two individuals, the 7 year-old (± 24 months) child from the single burial CG4, Loc. CR6:48 and the 4 year-old (+ 12 months) infant from the double Burial CG2, Loc. CR5:53, had one trait in common: Both showed multiple Wormian bones and a *sutura* mendosa. However, Wormian bones can also occur in diseases with particular tension forces affecting the growth of the cranium, such as *hydrocephalus*, or rare syndromes like *osteogenesis imperfecta* (Semler *et al.* 2010). Their presence in the two individuals could also be purely coincidental.

In Basta, epigenetic traits, particularly the high frequency (35.7%) of congenitally missing maxillary lateral incisors, were used to demonstrate very close familial relationships, possibly due to socio-cultural choices (Alt *et al.* 2013). In Ba`ja, none of the investigated individuals showed this particular trait.

Pathological Changes

Four out of eight individuals showed a pronounced porosity of the external lamina of the parietals near the lambdoid suture. In children, this type of porosity may be caused by anemia of various origins (Angel 1964; Ortner 2003; Gresky 2022), including malnutrition (*e.g.,* iron or vitamin B deficiency), chronic blood loss (trauma or parasites), or genetic diseases (beta thalassemia) (Herold 2000). Only the two pairs of individuals from the double Burials CG8, Loci C10:405-I/II and CG2, Loci CR5:53/54 were affected. Genetic investigations of individual Loc. C10:405-I revealed the presence of sickle cell anemia (Skourtanioti and Feldman this volume). Another individual, Loc. DR19:110, shows a lesser extent of porosity, which, based on differential diagnosis, could be attributed to physiological growth. Malnutrition in infants can arise from actual food scarcity or limited food resources, possibly provoked by a growing population in the village. It can also result from diseases that lead to malabsorption in the intestines, either being of infectious origin or caused by parasites. The parasitic load in early settlements could have been quite high, and in Ba`ja, with its restricted space of the settlement, it may have been even higher. In Basta, probable anemia was diagnosed in 13.3% of the non-adults (Schultz *et al.* 2004). At the PPN site of Shir in Syria, a high frequency of porosity of the external lamina was observed in non-adults, with 10 out of 19 individuals showing these changes. This high percentage could indicate poor hygiene conditions in the large settlement of Shir (Gresky in prep.). As anemia-causing genetic disease, thalassemia is frequently found. The earliest evidence of possible thalassemia in the Levant comes from Atilt-Yam in Israel, dating back to the Pre-Pottery Neolithic C, *c*. 6900-6300 cal BCE (Hershkovitz and Edelson 1991), but its origin might be even earlier.

Changes in the bone structure of the internal lamina can have various reasons. The irregular surface of the internal lamina, particularly in the frontal and parietal *tubera*, can be attributed to growth process, while thick layers of newly formed bone may indicate past hemorrhagic or inflammatory processes (Schultz 2003). Six out of eight non-adults showed changes of the internal lamina, suggesting a pathological process in four cases, which consisted of more or less remodeled new bone formations, in two of the older children only of remodeled bone formation. In Basta, changes of the internal lamina were quite frequently found, they occurred in 13.3% of the non-adults (Schultz *et al.* 2004). In the settlement of Shir, they were frequently found as well: 15 of 19 showed changes of the internal lamina (Gresky in prep).

Porosity of the orbital roof was observed in three out of seven individuals. This condition can be associated with various diseases such as anemia, rickets, or scurvy, and may also be related to changes in the external and internal lamina of the cranial vault. In Basta, cribra orbitalia was present in 4.5% of the non-adults (Schultz *et al.* 2004). In Shir, no cases of cribra orbitalia were found in eight younger infants with preserved orbital roofs. However, some of these young non-adults had already developed cranial porotic hyperostosis, indicating the onset of anemia. Four of the two children and three adolescents showed cribra orbitalia (Gresky *et al.* 2018).

The lack of caries and periapical processes in all individuals can be attributed to the generally young age of individuals in the sample. Caries and consecutive periapical processes accumulate over time and are more often found in adults. The lack of caries in non-adults is due to this fact and might also indicate a diet, predominantly not based on carbohydrates, which are known to create caries (Hillson 1996). In ‘Ain Ghazal, one child had caries (Rollefson *et al.* 1985) and 23% (n=3/13) of the older adult individuals. In Shir, caries was not found in infants and children but in three of six adolescents and adults (Gresky *et al.* 2018). In Basta, only the teeth of adults were investigated, and only a relatively low frequency of 9.1% (n=2/22) of the individuals showed dental caries. The diet in these four sites seemed to have been low in carbohydrates for both young individuals and possibly also adults. However, the severe dental wear often observed in adults might have contributed to a reduction in the occurrence of carious lesions.

Calculus might result of particular diets, but it is primarily determined by the oral milieu of the individual (Lieverse 1999). As it accumulates gradually over time, non-adults tend to

have only smaller amounts of calculus compared to older age groups. The individuals from Ba`ja, including the adult Loc. C10:408.8, showed only small amounts of calculus. However, it originated already at a young age, as evidenced by the presence of calculus in the 1.5 year-old infant (Loc. CR5:54). The small amount of calculus might also be due to the poor preservation, possibly calculus had been present in more severe extent. In Shir, the youngest individual with traces of calculus was 3-4 years old. In the older age group, all individuals (n=6/6) showed remnants of calculus (Gresky *et al.* 2018). Similarly, at ʻAin Ghazal, moderate to severe amounts of calculus were frequently found in adults (Rollefson *et al.* 1985). In Basta, the high amount of dental calculus in 79.2% (n=19/24) of the individuals is discussed to be the reason for subsequent periodontal disease, leading to dental abscesses and, ultimately, ante-mortem tooth loss (Schultz *et al.* 2007).

Dental wear can provide information about the composition of diets, whether they consist of softer or highly abrasive materials (Hillson 1996). It is also dependent on the individual's enamel quality, and of course, it is highly related to age. In our sample, age is less problematic as the majority of individuals are infants and children with only one young adult. The young adult shows irregular dental wear, with severe dental wear observed on the anterior teeth compared to the posterior. This suggests work-related use of the anterior teeth, which may be attributed to using the teeth as a third hand, *e.g.*, holding leather or other materials tightly between the teeth while processing it with the hands (*e.g.*, Larsen 1985). The difference in dental wear between the more used left side in contrast to the right side either points to an individual habit or might also be work-related. In relation to his age, the individual does not show very intense dental wear, as the adult and mature individuals from Basta had more severe dental wear (Schultz *et al.* 2007) as was also evidenced for the permanent molars of the individuals in Shkārat Msaied (Kinzel *et al.* 2017). In Shir, the only mature male showed an irregular pattern of severe wear, which could not originate from dietary attrition but rather from malocclusion or using teeth as tools. The non-adults in general show very little wear, with the mandibular incisors slightly more worn than the maxillary incisors (Gresky *et al.* 2018). Dental wear in the adults of ʻAin Ghazal was severe and attributed to the high content of abrasive particles in the food (Rollefson *et al.* 1985). The same reason was also discussed for the high amount of enamel chippings observed in the teeth of the individuals from ʻAin Ghazal (Rollefson *et al.* 1985).

Chipping of tooth enamel is influenced by factors such as the quality of enamel, which can vary among individuals, as well as by chewing hard substances, *e.g.*, small stones or nut shells that may be hidden components of food, predominantly affecting the molars and premolars (Turner and Cadien 1969). Chipping of the enamel of the anterior dentition might occur when biting hard materials, *e.g.*, cracking nuts or during work-related activities (Scott and Winn 2011). The adult individual (Loc. C10:408.8) shows enamel chippings on 10/18 teeth, mainly in the posterior dentition. This indicates the presence of hard substances within the food. Interestingly, the 7 year-old (± 24 months) individual, Loc. CR6:48, exhibits multiple small to deep chippings of enamel on seven teeth: four in the anterior dentition, three in the posterior dentition. In this case, it is not clear whether the multiple chippings are due to a weak enamel structure or excessive consumption of hard substances. In Shir, chipping of enamel was relatively rare. The youngest individual, aged 7-9 years, had multiple chippings, which could be attributed to cracking hard objects, such as almonds and pistachios that were a prominent part of the botanical sample of the site (Neef 2018).

Enamel hypoplasia represents a disturbance in enamel formation, which is attributed to periods of malnutrition or infectious disease during the developmental period of teeth (*e.g.*, Hillson 1996). Enamel hypoplasia predominantly forms in a linear pattern, but it can also occur in a spot-like manner. The occurrence of enamel hypoplasia can be related to the developmental ages during tooth formation (Ubelaker 1978). At Ba`ja, in the adult and in six out of twelve non-adults with preserved teeth, enamel hypoplasia was present, mainly in a linear form and ranging from faint to moderate degree. The most critical phase for their development was between 3 to 7 years of age. Together with the early deaths in the very young age group, it seems that the challenges encountered during early life were often fatal. There seems to be a notable period of stress between 3-5 years of age, during which many children either died or displayed evidence of a linear hypoplasia if they survived the stressful period. It might indicate a critical transition during weaning. Unfortunately, due to the lack

of collagen preservation, we were not able to observe a similar timing of weaning in C/N-isotope values. In Shir, eleven out of twelve individuals had enamel hypoplasia. More than half of the hypoplasia cases (52.4%) developed between the ages of 5 and 6 years which aligns with the age of occurrence observed in Ba`ja. This could suggest that a certain stress in this particular age meant a change of lifestyle for the children, which obviously was not easy. In Basta, quite a high number of individuals, 79.2% (n=19/24), had enamel hypoplasia. In ‘Ain Ghazal, even 91% (n=10/11) of the individuals experienced at least one episode of stress in childhood, with four individuals enduring repeated stress (Rollefson *et al.* 1985). For the Syrian Middle Euphrates Valley, the frequency of dental enamel hypoplasia was found to correlate with the level of economic and political stability in communities (Tomczyk *et al.* 2007). Additionally, it was influenced by transitions in subsistence patterns (Anfruns and Oms 2013), which arose from rapid population growth and settlement expansion, resulting in periodic food shortages and increased disease transmission.

Interproximal grooving, visible on the molars of Loc. C10:408.8, is known from adult dentitions from many sites and periods (*e.g.*, Lieverse *et al.* 2007; Gresky and Berezina 2022) and is discussed as a result of removing fibres from the interdental spaces by habitual use of toothpicks (*e.g.*, Ubelaker *et al*. 1969; Frayer 1991). It is attested for hunter-gatherers and agricultural groups, but it is rarely documented for the Neolithic period of the Near East. So far, there is one report of interproximal grooving in the population of Dja’de el-Mughara, Syria, 9th millennium BCE (Chamel *et al.* 2014). In Ba`ja, the lack of interproximal grooving of teeth might be due to the prevailing non-adult individuals, who did either not use tooth picks in young age or did not live long enough to show traces on their permanent dentition. However, in the few adult skeletons being found so far in Ba`ja, Loc. C10:408.8 is the only one displaying this particular feature, which might be connected to his special burial treatment in a single grave, in contrast to the other adults being buried in multiple burials (Benz *et al.* 2019).

In contrast to the high incidence of skull trauma in Basta, where 17.2% (n=5/29) of all individuals showed healed fractures (Schultz *et al.* 2007), there is no evidence of skull trauma in Ba`ja. Skull fractures are often a result of interpersonal violence, which seems to be common in Basta and associated with domestic conflicts within the community (Schultz *et al.* 2007). Although there are a few cases of trauma in Ba`ja, these can be rather attributed to accidents, as they affect a toe and a finger of two individuals. For ‘Ain Ghazal, Rollefson *et al.* (1985) describe a pattern of multiple injuries to the foot and ankle in adults, suggesting these injuries as a consequence of the steep terrain, in which the people lived.

In Ba`ja, the most severe trauma occurred in a 3 year-old child who had a fracture of at least two ribs, resulting in the development of pseudarthrosis. This injury could have been caused by an accidental fall or an intentional push. Furthermore, the presence of pseudarthrosis indicates that the infant did not receive adequate care or attention for proper healing of the fracture. In Shir, multiple symmetrical rib fractures were observed in a 6-12 month-old, possibly due to an underlying disease that led to a very porous bone structure. Additionally, three older individuals in Shir had two healed cranial fractures as well as a subcapital fracture of the second right metacarpal, suggesting interpersonal violence. Some fractures of the hand and feet are discussed as being of accidental nature (Gresky *et al.* 2018).

In Ba`ja, four individuals stood out due to distinct bone changes: two newborns showed flaring of the proximal ends of the long bones and sternal ends of ribs, which can be associated with deficiency diseases such as scurvy, rickets, or anemia (Ortner 2003; Gresky 2022). However, no additional signs of these diseases are present in the skeletons. A possible diagnosis of rickets could be discussed for a 3-4 year-old individual based on the severe bowing of the femoral shaft and flattened proximal humeri. Here as well, no further signs supporting the presence of rickets are observed. It might resemble a less severe episode of vitamin D deficiency that has already been survived, possibly due to prolonged periods spent in the dark, small houses as a result of another enduring illness (Brickley *et al.* 2020). In Basta, no cases of rickets were found, however, two cases of non-adult scurvy could be evidenced.

A very interesting case of a 3-4 year-old individual (Loc. CR5:54) from Ba`ja with very gracile appearance of all long bones of the upper and lower extremities can be explained

by a possible inactivity atrophy which might have been caused by a very long recovery phase after a disease or might even have been due to neurological disorders leading to a paralysis or other systemic diseases like poliomyelitis (Berner *et al.* 2021). This would implicate that the child was taken care of for a long time as it was not able to move (bioarchaeology of care, Tilley 2015).

Summary and Outlook

The 16 investigated individuals from Ba`ja comprised one adult, as well as 15 infants and children, who were buried in six single and three double burials, and in one small multiple burial. The five individuals who died between the ages of 3-4 years were all buried together with one individual of the youngest age group. The preservation of the bones is generally poor, being better in the younger individuals compared to the older ones. The majority of non-adults, 13 out of 15, died at a very young age (between 9.5 lunar months and 6-9 months and between 3-4 years of age). This may indicate a high infant mortality rate, but of course, this observation is strongly influenced by the burial customs, as mainly non-adults were buried within the settlement area. Furthermore, the analysis of the collective burials, in which adults were interred, was beyond the scope of this contribution since bones were either not available or analysis are ongoing and will be published elsewhere. Malnutrition and poor hygienic conditions, provoked by a growing population in the settlement, could be a reason for a high infant mortality. Pathological changes on the bones were observed in many individuals, albeit to a slight degree: anemia could be a possible diagnosis considering the porosity of the cranial vault and orbital roofs, as well as the flaring of the proximal ends of the long bones and sternal ends of ribs. Inflammatory changes of the internal lamina of the cranial vault are frequently observed. The frequency of dental diseases is limited due to the young age of the group, with only small amounts of calculus indicating poor oral hygiene, while chippings of enamel may suggest the consumption of hard substances.

The young adult shows irregular dental wear with particularly severe wear on the anterior teeth which suggests work-related use. As preliminary analyses of the other adults in Ba`ja show, the adult of this study is the only showing interproximal grooving of the molars.

Stress in early childhood started in Ba`ja at the age of 7 months with a peak between 3 and 7 years. This could be attributed to a change of lifestyle for children within this age group. A 3 year-old child experienced a severe fracture of the ribs with subsequent pseudarthrosis. The presence of multiple traumata seems to be mainly related to accidents, as there is no clear evidence of interpersonal violence.

In general, the infants and children from Ba`ja show similar burial customs and also disease patterns as individuals from contemporary sites in Jordan and Syria.

So far, the small number of individuals hinders further interpretation of the results. However, future research with a larger sample size would allow for more robust comparisons of disease frequencies and burial customs. The high number of non-adult individuals in Ba`ja promises a high potential for research, as their bones are much better preserved than those of the adults. In addition, advanced methods such as computed tomography and light microscopy will be utilised to aid in the diagnoses of diseases. Furthermore, the analysis of dental calculus holds great potential for detecting dietary patterns and identifying possible infectious agents, and will be employed in future investigations to gain a more comprehensive picture of the living conditions of the inhabitants from Ba`ja.

Acknowledgements

We are grateful to Katie White-Iribhogbe for taking part in the 2016 excavation, Juliane Dorn for taking pictures with the digital microscope and editing the skeletal schemes and figures, Julia Krauß for checking the non-metric dental traits, and all archaeologists for their enthusiasm and careful work.

Julia Gresky
Division of Natural Sciences
German Archaeological Institute, Berlin
julia.gresky@dainst.de

References

Acsádi G.Y. and Nemeskéri J.
1970 *History of human life span and mortality*. Budapest: Akadémiai Kiadó.

Alt K.W.
1997 *Odontologische Verwandtschaftsanalyse: individuelle Charakteristika der Zähne in ihrer Bedeutung für Anthropologie, Archäologie und Rechtsmedizin.* Stuttgart [u.a.]: Fischer.

Alt K.W., Benz M., Müller W., Berner M.E., Schultz M., Schmidt-Schultz T.H., Knipper C., Gebel H.G.K., Nissen H.J. and Vach W.
2013 Earliest evidence for social endogamy in the 9,000-year-old-population of Basta, Jordan. *PLoS ONE* 8(6): e65649. doi: 10.1371/journal.pone.0065649

Alt K.W., Benz M., Vach W., Tal L. Simmons and Goring-Morris A.N.
2015 Insights into the social structure of the PPNB site of Kfar HaHoresh, Israel, based on dental remains. *PLoS ONE* 10(9): e0134528. doi: 10.1371/journal.pone.0134528

Anfruns J. and Oms J.I.
2013 Antropología y paleopatología dentarias de la población neolítica de Tell Halula. In: M. Molist Montaña (ed.), *Tell Halula: un poblado de los primeros agricultores en el valle del Éufrates, Siria*: 450-470. Barcelona: Ministerio de Educación, Cultura y Deporte.

Angel J.L.
1964 Osteoporosis: thalassemia? *American Journal of Physical Anthropology* 22: 369-374.

Baker O., Lee O.-Y., Wu H.H.T., Besra G.S., Minnikin D.E., Llewellyn G., Williams C.M. *et al.*
2015 Human Tuberculosis predates domestication in ancient Syria. *Tuberculosis* 95: S4-12. doi: 10.1016/j.tube.2015.02.001

Balasse M., Al Zaidaneen J.S., Dean R.M., Price T.D. and Henry D.O.
2014 Tracing herding patterns at Ayn Abū Nukhayla through biogeochemical analyses (^{13}C, ^{18}O, $^{87}Sr/^{86}Sr$) in faunal remains. In: D.O. Henry and J.E. Beaver (eds.), *The sands of time. The desert Neolithic settlement at Ayn Abū Nukhayla*. bibliotheca neolithica Asiae meridionalis et occidentalis: 91-104. Berlin: ex oriente.

Bartl K.
2018 Site and setting. In: K. Bartl (ed.), *The Late Neolithic site of Shir / Syria. The excavations at the South Area 2006-2009.* Damaszener Forschungen 18: 13-34. Darmstadt: wbg, Philipp von Zabern.

Benz M., Alarashi H., Gresky J., Purschwitz C. and Gebel H.G.K.
2023 Moments of memory and belonging. A special child burial from Neolithic Ba`ja, Southern Jordan. In: E. Murphy and M. Le Roy (eds.), *Normative, atypical or deviant? Interpreting prehistoric and protohistoric child burial practices*: 10-31. Oxford: Archaeopress.

Benz M., Gresky J. and Alarashi H.
2020 Similar but different. Displaying social roles of subadults in burials from the Late Pre-Pottery Neolithic Site of Ba`ja, Southern Jordan. In: H. Alarashi and R.M. Dessì (eds.), *L'art du paraître apparences de l'humain, de la préhistoire à nos jours. The art of human appearance: from prehistory to the present day. 40e rencontres internationales d'archéologie et d'histoire* – Nice Côte d'Azur: 93-107. Nice: APDCA.

Benz M., Gresky J., Štefanisko D., Alarashi H., Knipper C., Purschwitz C., Bauer J. and Gebel H.G.K.
2019 Burying power: New insights into incipient leadership in the Late Pre-Pottery Neolithic from an outstanding burial at Ba'ja, southern Jordan. *PLoS ONE* 14(8): e0221171.

Berner M., Pany-Kucera D., Doneus N., Sladek V., Gamble M. and Eggers S.
2021 Challenging definitions and diagnostic approaches for ancient rare diseases: the case of Poliomyelitis. *International Journal of Paleopathology* 33: 113-127. doi: 10.1016/j.ijpp.2021.04.003

Brickley M., Ives R. and Mays S.
2020 *The bioarchaeology of metabolic bone disease* 2. San Diego: Elsevier.

Brothwell D.R.
1981 *Digging up bones: the excavation, treatment, and study of human skeletal remains.* Ithaca: Cornell University Press.

Buikstra J.E. and Ubelaker D.H. (eds.)
1994 *Standards for data collection from human skeletal remains*. Archeological Survey Research Series 44. Fayetteville: Arkansas.

Chamel B., Ravy E. and Coqueugniot E.
2014 *Task related wear, interproximal grooves and*

non-masticatory tooth use in the Pre-Pottery Neolithic population of Dja'de el-Mughara (Syria, 9th millennium BC). 9. International Congress on the Archaeology of the Ancient Near East. June 9-13, 2014: 28. University of Basel. n.d.

Drenhaus U.
1992 Methoden der Paläodemographie. In: R. Knussmann (ed.), *Anthropologie: Handbuch der Vergleichenden Biologie des Menschen* 1: 602-616. Stuttgart, New York: Fischer.

Dupont C., Armant D.R. and Brenner C.A.
2009 Epigenetics: definition, mechanisms and clinical perspective. *Seminars in Reproductive Medicine* 27(5): 351-357. doi: 10.1055/s-0029-1237423

Edgar H.
2017 *Dental morphology for anthropology: an illustrated manual*. New York: Routledge.

El-Najjar M., Al-Shiyab A. and Al-Sarie I.
1996 Cases of Tuberculosis at 'Ain Ghazal, Jordan. *Paléorient* 22(2): 123-128. doi: 10.3406/paleo.1996.4639

Fazekas I.G. and Kósa F.
1978 *Forensic fetal osteology*. Budapest: Akadémiai Kiadó.

Feldman M., Fernández-Domínguez E., Reynolds L., Baird D., Pearson J., Hershkovitz I., May H., *et al.*
2019 Late Pleistocene human genome suggests a local origin for the first farmers of Central Anatolia. *Nature Communications* 10(1): 1218. doi: 10.1038/s41467-019-09209-7.

Ferembach D., Schwidetzky I. and Stloukal M.
1979 Empfehlungen für die Alters- und Geschlechtsdiagnose am Skelett. *Homo* 30: 1-32.

Florkowski A. and Kozłowski T.
1994 Ocena wieku szkieletowego dzieci na podstawie wielkosci kosci. *Przeglad Antropologiczny* 57: 1-2, 71-86.

Frayer D.W.
1991 On the etiology of interproximal grooves. *American Journal of Physical Anthropology* 85: 299-304.

Gebel H.G.K., Nissen H.J. and Zaid Z. (eds.) with a contribution by M. Kinzel
2006 *Basta II. The architecture and stratigraphy.* bibliotheca neolithica Asiae meridionalis et occidentalis, Monograph of the Faculty of Archaeology and Anthropology 5. Berlin: ex oriente.

Gresky J.
2022 Metabolische Erkrankungen, Mangelernährung und unspezifische Infektionen. In: J. Weber, J. Wahl and A. Zink (eds.), *Osteologische Paläopathologie. Ein bebildertes Lehrbuch mit medizinischen Anmerkungen*: 389-430. Berlin: Lehmanns.
in prep Microscopic analyses on non-adult bones from Neolithic Shir, Syria.

Gresky J. and Berezina N.
2022 Anthropological characteristics of the individuals. In: A.A. Kalmykov, A.B. Belinskij, S. Hansen, S. Reinhold and K. Hellström (eds.), *Der bronzezeitliche Großgrabhügel der Nekropole Rasševatskij-1 in der Steppe des Vorkaukasus.* Archäologie in Eurasien 41: 187-241.

Gresky J., Haelm J., Resch D. and Bartl K.
2018 Anthropological and paleopathological investigations. In: K. Bartl (ed.), *The Late Neolithic site of Shir / Syria. The excavations at the South Area 2006-2009.* Damaszener Forschungen18: 633-687. Darmstadt: wbg, Philipp von Zabern.

Grindell B.
1998 *Unmasked equalities: an example of mortuary practices and social complexity in the Levantine Natufian and Pre-Pottery Neolithic*. Ann Arbor: University of Arizona, University Microfilms. PhD Thesis.

Hauser G. and DeStefano G.F.
1989 *Epigenetic variants of the human skull*. Stuttgart: Schweizerbart'sche Verlagsbuchhandlung.

Hermansen B.D., Thuesen I., Jensen C.H., Kinzel M., Petersen M.B., Schjellerup Jørkov M.L. and Lynnerup N.
2006 Shkarat Msaied: the 2005 season of excavations. A short preliminary report. *Neo-Lithics* 1/06: 3-7.

Herold G.
2000 *Innere Medizin. Eine vorlesungsorientierte Darstellung*. Köln: Herold.

Hershkovitz I. and Edelson G.
1991 The first identified case of thalassemia? *Human Evolution* 6(1): 49-54. doi: 10.1007/BF02435606

Hershkovitz I., Donoghue H.D., Minnikin D.E., Besra G.S., Lee O.Y., Gernaey A.M., Galili E., Eshed V., Greenblatt C.L., Lemma E., Bar-Gal G.K. and Spigelman M.
2008 Detection and molecular characterization of 9,000-year-old Mycobacterium tuberculosis

from a Neolithic settlement in the Eastern Mediterranean. *PLoS One* 3: e3426.

Hillson S.
1996 *Dental anthropology*. Cambridge: Cambridge University Press.

Itahashi Y., Tsuneki A., Dougherty S.P., Chikaraishi Y., Ohkouchi N. and Yoneda M.
2018 Dining together: reconstruction of Neolithic food consumption based on the $\delta^{15}N$ values for individual amino acids at Tell el-Kerkh, Northern Levant. *Journal of Archaeological Science* 17: 775-784.

Kinzel M., Jørkov M.L., Stråhlén R., Thuesen M.B. and Thuesen I.
2017 Shkārat Msaied 2016: new results from Unit F. *Neo-Lithics* 01/2017: 13-17.

Larsen C.S.
1985 Dental modifications and tool use in the western Great Basin. *American Journal of Physical Anthropology* 67: 393-402.

Lieverse A.R.
1999 Diet and the aetiology of dental calculus. *International Journal of Osteoarchaeology* 9(4): 219-232.

Lieverse A.R., Link D.W., Bazaliiskiy V.I., Goriunova O.I. and Weber A.W.
2007 Dental health indicators of hunter-gatherer adaptation and cultural change in Siberia's Cis-Baikal. *American Journal of Physical Anthropology* 134(3): 323-339. doi: 10.1002/ajpa.20672

López-González F., Grandal-d'Anglade A. and Vidal-Romaní J.R.
2006 Deciphering bone depositional sequences in caves through the study of manganese coatings. *Journal of Archaeological Science* 33(5): 707-717. doi: 10.1016/j.jas.2005.10.006

Mann R.W., Hunt D.R. and Lozanoff S.
2016 *Photographic regional atlas of non-metric traits and anatomical variants in the human skeleton.* Springfield: Thomas.

Neef R.
2018 Palaeobotanical remains. In: K. Bartl (ed.), *The Late Neolithic site of Shir / Syria. The excavations at the South Area 2006-2009.* Damaszener Forschungen 18: 688-695. Darmstadt: wbg, Philipp von Zabern.

Nissen H.J., Muheisen M. and Gebel H.G.K. (eds.)
2004 *Basta I. The human ecology.* bibliotheca neolithica Asiae meridionalis et occidentalis and Yarmouk University, Monograph of the Faculty of Archaeology and Anthropology 4. Berlin: ex oriente.

Ortner D.J.
2003 *Identification of pathological conditions in human skeletal remains*. New York: Academic Press.

Perizonius W.R.K. and Pot T.J.
1981 Diachronic dental research on human skeletal remains excavated in the Netherlands 1: Dorestad's cemetery on the Heul. *Berichten van de Rijksdienst voor het Oudheidkundig Bodemonderzoek* 31: 369-413.

Perry M.A.
2012 Paleopathology in Lebanon, Syria, and Jordan. In: J. Buikstra and C. Roberts (eds.), *The global history of paleopathology*: 451-469. Oxford: Oxford University Press. doi: 10.1093/acprof:osobl/9780195389807.003.0049

Phenice T.W.
1969 A newly developed visual method for sexing the os pubis. *American Journal of Physical Anthropology* 30: 297-302.

Resch D. and Gresky J.
2018 Burials and burial customs. In: K. Bartl (ed.), *The Late Neolithic site of Shir / Syria. The excavations at the South Area 2006-2009.* Damaszener Forschungen 18: 603-632. Darmstadt: wbg, Philipp von Zabern.

Richter T., Bocaege E., Ilsøe P., Ruter A., Pantos A., Pedersen P. and Yeomans L.
2019 Ochre, ground stone, and wrapping the dead in the Late Epipalaeolithic (Natufian) Levant: revealing the funerary practices at Shubayqa 1, Jordan. *Journal of Field Archaeology* 44(7): 440-457. doi: 10.1080/00934690.2019.1645546.

Rollefson G.O., Simmons A., Donaldson M., Gillespie W., Kafafi Z., Köhler-Rollefson I., McAdame E., Rolston S. and Tubb K.
1985 Excavations at the PPNB village of 'Ain Ghazal (Jordan) 1983. *Mitteilungen der Deutschen Orient Gesellschaft* 117: 69-116.

Santana J., Millard A., Ibáñez-Estevez J.J., Bocquentin F., Nowell G., Peterkin J., Macpherson C., Muñiz J., Anton M., Alrousan M. and Kafafi Z.
2021 Multi-isotope evidence of population aggregation

in the Natufian and scant migration during the early Neolithic of the Southern Levant. *Scientific Reports* 11: 11857. doi: 10.1038/s41598-021-90795-2

Scheuer L. and Black S.
2000 *Developmental juvenile osteology*. Elsevier. doi: 10.1016/B978-0-12-624000-9.X5000-X

Schultz M.
1988 Methoden der Licht- und Elektronenmikroskopie. In: R. Knußmann (ed.), *Anthropologie. Handbuch der vergleichenden Biologie des Menschen* 1, 1: 698-730. Stuttgart, New York: Fischer.
2003 Light microscopic analysis in skeletal paleopathology. In: D.J. Ortner (ed.), *Identification of pathological conditions in human skeletal remains.* New York: Academic Press.

Schultz M. and Schmidt-Schultz T.H.
2019 Health and disease in the prehistoric and early historical Near East: a contribution to the reconstruction of ancient living conditions. In: J. Becker, C. Beuger and B. Müller-Neuhof (eds.), *Human iconography and symbolic meaning in Near Eastern Prehistory: proceedings of the workshop held at 10th ICAANE in Vienna, April 2016.* OREA 11: 25-56. Wien: Austrian Academy of Sciences Press.

Schultz M., Berner M. and Schmidt-Schultz T.H.
2004 Preliminary results on the morbidity and mortality in the Late PPNB population of Basta, Jordan. In: H-D. Bienert and H.G.K. Gebel (eds.), *Central settlements in Neolithic Jordan.* Studies in Early Near Eastern Production, Subsistence, and Environment 5: 259-270. Berlin: ex oriente.

Schultz M., Schmidt-Schultz T.H., Gresky J., Kreutz K. and Berner M.
2007 Morbidity and mortality in the Late PPNB populations from Basta and Ba'ja (Jordan). In: M. Faerman, L.K. Horwitz, T. Kahana and U. Zilberman (eds.), *Faces from the past: diachronic patterns in the biology of human populations from the Eastern Mediterranean: papers in honour of Patricia Smith*. BAR international series 1603: 82-99. Oxford: Archaeopress.

Schwörer I.
1975 *Die Skelettentwicklung des Menschen, Lehrtafel.* Stuttgart: Thieme.

Scott G.R. and Winn J.R.
2011 Dental chipping: contrasting patterns of microtrauma in Inuit and European populations. *International Journal of Osteoarchaeology* 21(6): 723-731.

Semler O., Cheung M.S., Glorieux F.H. and Rauch F.
2010 Wormian bones in osteogenesis imperfecta: correlation to clinical findings and genotype. *American Journal of Medical Genetics Part A* 152A: 1681-1687.

Shewan L.
2004 Natufian settlement systems and adaptive strategies: the issue of sedentism and the potential of strontium isotope analysis. In: C. Delage (ed.), *The last hunter-gatherers in the Near East.* BAR international series 1320: 55-94. Oxford: Archaeopress.

Simmons A.
2007 *The Neolithic revolution in the Near East. Transforming the human landscape*. Tucson: University of Arizona Press.

Sjøvold T.
1988 Geschlechtsdiagnose am Skelett. In: R. Knußmann (ed.), *Anthropologie. Handbuch der vergleichenden Biologie des Menschen* 1, 1: 444-480. Stuttgart, New York: Fischer.

Smith P., Bar-Yosef O. and Sillen A.
1984 Archaeological and skeletal evidence for dietary change during the late Pleistocene/ early Holocene in the Levant. In: M.N. Cohen and G.J. Armelagos (eds.), *Paleopathology at the origins of agriculture*: 101-136. Gainesville: University Press of Florida.

Tilley L.
2015 *Theory and practice in the bioarchaeology of care.* Cham: Springer International Publishing. doi: 10.1007/978-3-319-18860-7

Tomczyk J., Sołtysiak A. and Tomczyk-Gruca M.
2007 Temporal changes in frequency of enamel hypoplasia in the Middle Euphrates Valley (Syria). In: E.B. Bodzsár and A. Zsákai (eds.), *Human diversity and biocultural researches, selected papers of the 15th Congress of the European Anthropological Association*. Humanbiologia Budapestinensis 30: 87-89. Budapest: Department of Biological Anthropology.

Turner C.G. and Cadien J.D.
1969 Dental chipping in Aleuts, Eskimos and Indians. *American Journal of Physical Anthropology* 31(3): 303-310. doi: 10.1002/ajpa.1330310305

Ubelaker D.H.
1978 *Human skeletal remains: excavation, analysis, interpretation*. Chicago: Aldine.

Ubelaker D.H., Phenice T.W. and Bass W.M.
1969 Artificial interproximal grooving of the teeth in American Indians. *American Journal of Physical Anthropology* 30: 145-150.

Vallois H.V.
1937 La durée de la vie chez l'homme fossile. *L'Anthropologie* 47: 499-532.

Wang X., Skourtanioti E., Benz M., Gresky J., Ilgner J., Lucas M., Morsch M., Peters J., Pöllath N., Ringbauer H. *et al.*
2023 Isotopic and DNA analyses reveal multiscale PPNB mobility and migration across Southeastern Anatolia and the Southern Levant. *PNAS* 120(4) e2210611120. doi: 10.1073/pnas.2210611120

Appendix 1: Catalogue

The description of human remains follows the order of the description of the burials. It starts in Area C in the east and proceeds to Area D towards the west.[1] The skeletal inventory diagrams provide an overview of the bones available for investigation. The dark grey colour indicates preserved bones, while the light grey colour indicates fragmentary bones. A star next to a bone in the inventory indicates that this element could also be from the opposite side of the body.

Above each skeleton, the dental inventory diagram is situated. Depending on the age group, deciduous and/ or permanent dentitions are presented, with the existing teeth marked in dark grey. The counting of the teeth is based on the FDI scheme (see Materials and Methods).

The labeling of the figures in the catalogue, *e.g.*, Fig. S53-2 is composed of the following elements: S = supplementary, 53 = locus number (CR5:53), and -2 = consecutive number of the figure in one individual.

Photos and radiographs: J. Gresky, Ba`ja N.P., DAI, drawings: J. Dorn, DAI.

[1] Investigations on the collective Burials CG1, CG11-12, and DG1 are ongoing and will be reported elsewhere. Preliminary results of the morphological analyses on the human remains from collective Burial CG1 by Susan Klingner are given in Benz *et al.* this volume Part 2: Appendix 3 to this contribution. Italics are not used for Latin terms in this catalogue, because of their high frequency and to improve readability.

CR5:53, CR5:54

Double Burial CG2

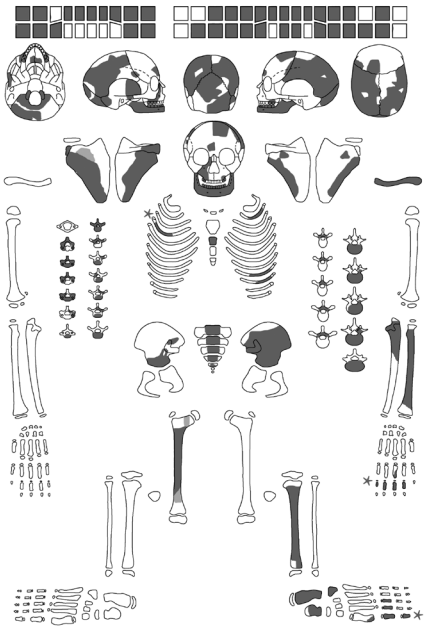

Individual CR5:53

A. Skeletal data

Preservation: Bone surface: severely eroded, many plant roots, many black spots
Bone consistency: very fragile
Completeness: 50% preserved
Age: 4 years (+ 12 months)
Dental development: 4-5 years
The size of the mandible is quite small for the age of 4 years.
The parietal bones are shortened in sagittal direction, with the left parietal basis measuring approximately 75mm.
Clavicle left length: 64mm, straight shape
Radius left length: approximately 95mm
Radius left transverse mid-shaft diameter: 6mm
Ilium left height: 52mm
Ilium left width: approximately 57mm
Femur right length: minimum 140mm
Femur right circumference: 32mm
Tibia left length: minimum 129mm
Tibia left sagittal diameter at the mid-shaft: 9mm
Tibia left transverse diameter at the mid-shaft: 8mm
Calcaneus left length: 28mm
Sex: female > male
Mandible: prominent mental protuberance
Pelvis: left side with wide sciatic notch and prominent preauricular sulcus
Very gracile and thin bones

B. Pathological data

1. Cranium and mandible

Ectocranial surface: At least 11 Wormian bones are present within the lambdoid and sagittal sutures (Figs. S53-1, S53-2). Sutura mendosa on both sides of the occipital (Fig. S53-3), approximately 35mm long. Another suture, located 10mm superior of it, runs parallel to the sutura mendosa. On the right side, the adjacent parts are missing, on the left side, the suture is connected to a lambdoid ossicle (Fig. S53-2). Both parietals show a porous surface close to the lambdoid sutures (Fig. S53-2).
Endocranial surface of the cranial base: The surfaces of the anterior fossa and the squama temporalis show whitish porous bone formations (Fig. S53-4).
Orbital roof: The right orbital roof shows a small blood vessel impression, which is surrounded by a fine porous 5 x 2mm area (Figs. S53-5, S53-6).
Dentition, alveolar region, and temporomandibular joints: The surface of the inferior half of the mandible in the area of the incisors is porous. Deciduous dentition: calculus: teeth 54, 63 (grade I), teeth 55, 64-65 (grade II). Attrition of the anterior dentition (grade 4-4+) and posterior dentition (grade [3] 4-5). Transverse lines on the roots of teeth 55, 65, 63 (Fig. S53-7).
Permanent dentition (not erupted yet): Transverse linear enamel hypoplasia on teeth 15-16, 25 (grade I) and 11-14, 21-24, 33-34 (grade II) (Figs. S53-8, S53-9): *c*. 3 years ± 12 months, 4 years ± 12 months. Spot-like enamel hypoplasia on tooth 11: *c*. 1 year ± 4 months.

2. Post-cranial skeleton

Distal upper limb: The radius and ulna are particularly thin for their lengths (Figs. S53-10 to S53-13).
Proximal and distal lower limbs: The femur and tibia are particularly thin for their lengths.
Foot: The distal phalanx of the first left digit shows a fissure of its distal end. It is V-shaped including a small foramen (Figs. S53-14 to S53-16).

3. Probable diagnosis of selected disease types
Morphological variation/ developmental disorder: At least 11 Wormian bones are present within the lambdoid and sagittal sutures. Sutura mendosa present on both sides. V-shaped distal joint surface of the distal phalanx of the left first toe. Possible atrophy caused by inactivity of the upper and lower limbs.

Fig. S53-1
Posterior view on the occipital and parietal bones showing at least 11 Wormian bones within the lambdoid and sagittal sutures.

Fig. S53-2
External surface of the left parietal bone with porous surface near the lambdoid suture and an additional suture (arrows) connected to a lambdoid ossicle (stars).

Fig. S53-3 Internal lamina of the inferior part of the occipital bones with a sutura mendoza (arrow).

Fig. S53-4
The internal lamina of the right squama temporalis shows porous whitish bone formations.

Fig. S53-5
The right orbital roof shows a small blood vessel impression surrounded by a fine porous area of 5 x 2mm.

Fig. S53-6 Detail of the fine porous 5 x 2mm area on the right orbital roof (*Hirox KH-870031*).

Fig. S53-7
Tooth 63 with transverse lines on the root and small remnants of calculus on the crown.

Fig. S53-8
Labial surface of tooth 12 showing transverse linear enamel hypoplasia.

Fig. S53-9
Lingual surface of tooth 12 showing shoveling.

Fig. S53-10
Fragment of the left radius (star) compared to a healthy right radius of an individual of the same age.

Fig. S53-11
Fragment of the right femur (star) compared to a healthy left femur of an individual of the same age.

Fig. S53-12
Fragment of the left tibia (star) compared to a healthy right tibia of an individual of the same age.

Fig. S53-13
Radiograph of postcranial elements anterior-posterior, 70kV 5min, 3mAs.

Fig. S53-14
Dorsal view of the distal phalanx of the first left digit showing a fissure of its distal end.

Fig. S53-15
Palmar view of the distal phalanx of the first left digit showing a fissure of its distal end.

Fig. S53-16
Distal joint surface of the distal phalanx of the first left digit with a V-shaped fissure that includes a small foramen.

Individual CR5:54

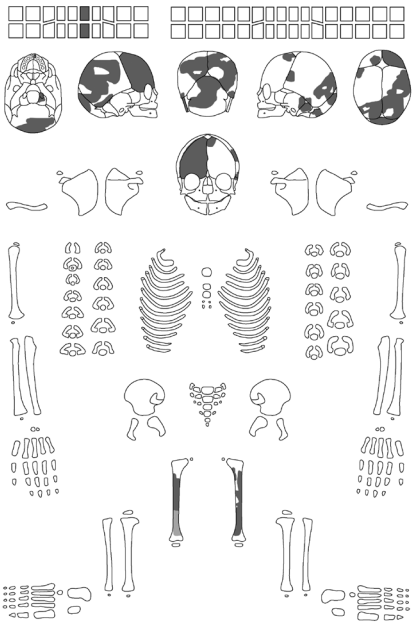

A. Skeletal data

Preservation: Bone surface: good, black spot-like colouration, red pigment on the external lamina of the right frontal bone
Bone consistency: fragile
Completeness: 10% preserved
Age: 18 months
Anterior fontanel not yet closed
Dental development (length of teeth roots): 18 months
Femur both length (fragment): 83mm
Femur both circumference: 22mm
Sex: indeterminable

B. Pathological data

1. Cranium and mandible

Ectocranial surface: Porous surface on the right parietal bone close to the lambdoid suture (Fig. S54-1).
Endocranial surface: The surface of the impressiones digitatae of the frontal (Fig. S54-2) bone shows whitish porous bone formations. There are more additional small blood vessel impressions visible on the left parietal bone compared to the right. The occipital bone exhibits lingulate, plaque-like new bone formations next to the confluens sinuum on both sides (Fig. S54-3).
Endocranial surface of the cranial base: The surface of the right anterior fossa shows whitish porous bone formations.
Dentition, alveolar region, and temporomandibular joints: calculus: tooth 71 (grade I). Attrition of the anterior dentition (grade 2).

2. Post-cranial skeleton

Proximal lower limb: Both femora have thin cortical bone.

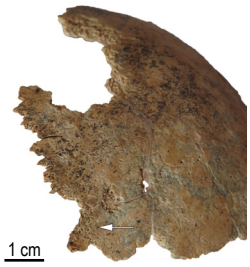

Fig. S54-1
Posterior view of the right parietal bone with porous surface (arrow) near the lambdoid suture.

Fig. S54-2
Internal lamina of the right frontal bone with porous whitish bone formations in the impressiones digitatae.

Fig. S54-3
Internal lamina of the squama occipitalis with lingulate, plaque-like new bone formations next to the confluens sinuum on both sides (arrows).

CR5:49A

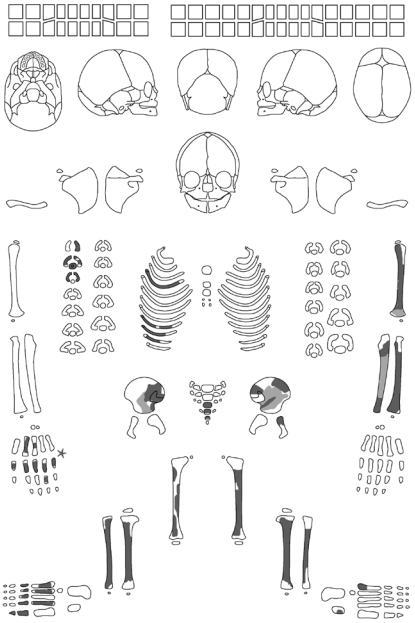

Single Burial CG3

A. Skeletal data

Preservation: Bone surface: eroded, all dark on the external side, lighter on the internal surface
Bone consistency: very fragile
Completeness: 30% preserved
Age: 1.5-2 years
Humerus left length: minimum 110mm
Radius left length: minimum 79mm
Femur left length: minimum 140mm
Tibia left length: minimum 125mm
Sex: indeterminable

B. Pathological data

2. Post-cranial skeleton

Rib cage: There are two notches on the inferior rim of the 10th right rib in the region of the angulus (Figs. S49A-1, S49A-2).

Fig. S49A-1
Internal surface of the 10th right rib with two notches (arrow) on the inferior rim in the region of the angulus.

Fig. S49A-2
External surface of the 10th right rib.

CR6:48

Single Burial CG4

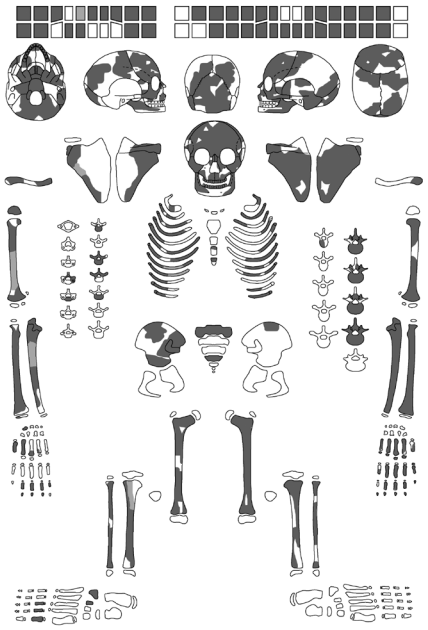

A. Skeletal data

Preservation: Bone surface: eroded
Bone consistency: very fragile
Completeness: 90% preserved
Age: 7 years (± 24 months)
Dental development: 6-8 years (± 24 months)
Scapula left width: 58mm
Radius right length: 131mm
Femur left length: 242mm
Tibia right length: 193mm
Tibia left length: 194mm
Sex: female >= male
Very gracile bones

B. Pathological data

1. Cranium and mandible

Ectocranial surface: One Wormian bone is present at the lambda (Fig. S48-1). The sutura mendosa is visible on the left occipital bone (Fig. S48-1), and there is a small remnant of the metopic suture cranial next to the glabella.
Endocranial surface: The surface of the caudal third of the frontal bones shows whitish very faint porous bone formations in the impressiones digitatae. On the lateral region of the right more than the left frontal bones there are small roundish pit-like impressions (Fig. S48-2).
Endocranial surface of the cranial base: The surface of the anterior fossa shows whitish very faint porous bone formations. The lateral region of the right frontal bones is more affected than the left side, there are shallow small roundish pit-like impressions. There are whitish thick porous bone formations, especially in the impressions of the cranial base, in the middle more than in the posterior fossae (Fig. S48-3).
Cranial sulci: The surface of the superior sagittal sulcus shows a 20mm long whitish porous plate-like bone formation close to the bregma.
Mastoid cells: Both mastoid processes have sufficiently pneumatised cells.
Orbital roof: Both orbital roofs show a fine porous surface, which might resemble physiological growth.
Nasal aperture: The surface of the floor and lateral walls on both sides are porous with reticulated vascular impressions which might resemble physiological growth.
Paranasal sinuses: The surface of the right maxillary sinus is porous in its anterior and middle part.
Dentition, alveolar region, and temporomandibular joints: Deciduous dentition: calculus: teeth 53, 64-65, 81-82 (grade I). Attrition of the anterior and posterior dentition (grade 4-5) (tooth 65, Fig. S48-4). Multiple small chippings of enamel on teeth 53, 61, 63, 64, 75, 84, and a deeper one on 63. Permanent dentition: calculus: tooth 31 (grade I), tooth 41 (grade II). Attrition of the anterior and posterior dentition (grade 1-2). Transverse linear enamel hypoplasia on teeth 14-15, 24-25, 31, 37, 41 (grade I) and 12-13, 22-23, 32-35 (tooth 32, Fig. S48-5), 42-45 (grade II): *c.* 3 years ± 12 months, 4 years ± 12 months, 5 years ± 16 months, 6 years ± 24 months, 7 years ± 24 months. Spot-like enamel hypoplasia on tooth 44: *c*. 3 years ± 12 months. Transverse lines on the roots of teeth 36 (Fig. S48-6) and 46.

2. Post-cranial skeleton

Rib cage: The lower rims of the right 8^{th}-11^{th} ribs in the region of the angulus have an extension to the inferior (Figs. S48-7 to S48-9). In this area the inner surface has a porous appearance.
Proximal upper limb: Both humeri show a foramen supratrochleare with multiple 1-2mm large shallow foramina distal and mesial to it (Fig. S48-10). The left humerus has a 4 x 4mm area with porous surface on its medial side *c.* 5mm distal of the proximal epiphyseal plate (Fig. S48-11).

Hand: The ulnar condyle of the distal joint of the middle phalanx in the second right digit is flattened, and there is a slight enlargement with small foramina in a row on its dorsal surface. These characteristics may resemble those of a well healed fracture (Figs. S48-12, S48-13).
Proximal lower limb: Both femora have a *c.* 16 x 10mm area with porous surface on their ventral surface of their neck (Fig. S48-14). The right femur shows faint Harris lines in its broken distal end.
Distal lower limb: The left tibia shows three Harris lines in its broken distal end (Fig. S48-15), while in the distal part of the right tibia, they are less clearly expressed.
Multiple Harris lines are visible in all long bones in their distal more than their proximal ends (Figs. S48-16, S48-17).

3. Probable diagnosis of selected disease types

Morphological variation/ developmental disorder: Wormian bone in lambda suture. Sutura mendosa left occipital, remnants of metopic suture cranial to glabella. Foramen supratrochleare on both humeri.
Trauma: Well healed fracture of the distal end of the middle phalanx of the second right digit.

Fig. S48-1 Posterior view of the occipital and both parietal bones, showing one Wormian bone (star) at the lambda. On the left occipital bone, a sutura mendosa is visible (arrow).

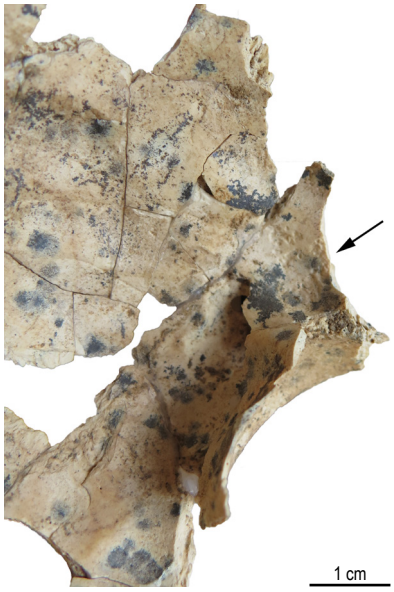

Fig. S48-2
Internal lamina of the right frontal bone with whitish, very faint porous bone formations in the impressiones digitatae and small roundish pit-like impressions (arrow).

Fig. S48-3
Internal lamina of the right ala major ossis sphenoidalis with whitish, thick, porous bone formations.

Fig. S48-4
Occlusal surface of tooth 65 with severe dental wear.

Fig. S48-5
Labial surface of tooth 32 with transverse linear enamel hypoplasia.

Fig. S48-6
Distal surface of tooth 36 with transverse lines on the roots.

Fig. S48-7
Internal surface of the right 8th-12th ribs.

Fig. S48-8 Internal surface of the 9th right rib, showing an extension of the surface to the inferior with a porous appearance.

Fig. S48-9 Internal surface of the 10th right rib, showing an extension of the surface to the inferior with a porous appearance.

Fig. S48-10
Anterior view of the distal part of the left humerus with a foramen supratrochleare.

Fig. S48-11
Anterior view of the proximal part of the left humerus, with a 4 x 4mm area showing porous surface on its neck (arrow).

Fig. S48-12
Dorsal view on the ulnar condyle of the distal joint of the middle phalanx in the second right digit. The condyle is flattened, and there is a slight enlargement with small foramina in a row on its dorsal surface (arrow).

Fig. S48-13
Palmar view on the ulnar condyle of the distal joint of the middle phalanx in the second right digit.

Fig. S48-14
Anterior view of the right femur with a porous surface on the neck (arrow).

Fig. S48-15
Internal surface of the broken distal end of the left tibia with five Harris lines.

Fig. S48-16 Radiograph of the upper extremity anterior-posterior, 70kV 7min, 3mAs. Multiple Harris lines are visible in all long bones, more pronounced in their distal than in their proximal ends.

Fig. S48-17 Radiograph of the lower extremity in an anterior-posterior view, 70kV 7min, 3mAs. Multiple Harris lines are visible in all long bones, more pronounced in their distal ends than in their proximal ends.

CR6:23a-b

Double Burial CG5

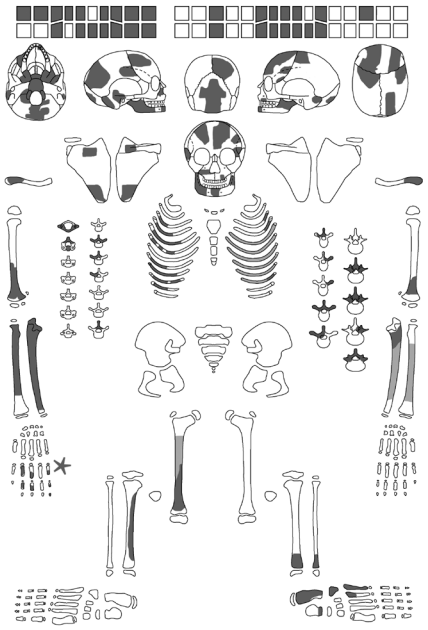

CR6:23a

A. Skeletal data

Preservation: Bone surface: eroded, red spot-like colouration and dark stripes, particularly on the right parietal bone
Bone consistency: fragile
Completeness: 40% preserved
Age: 3 years (+ 12 months)
Dental development, height of crowns of teeth 11, 12, 16, 21, 26 point to 3 years +12 months rather than -12 months
Pars basilaris ossis occipitalis length: 23mm
Pars basilaris ossis occipitalis width: 24.4mm
Radius right length: minimum 93mm
Sex: indeterminable

B. Pathological data

1. Cranium and mandible

Endocranial surface of the cranial base: The surfaces of the right ala major (Fig. S23a-1), the posterior fossa of the right occipital as well as the transverse and sigmoid sinus show porous bone formations.
Dentition, alveolar region, and temporomandibular joints: Deciduous dentition: Attrition of the anterior dentition (grade 1-2+) and posterior dentition (grade 1). Permanent dentition (partly not erupted yet): Transverse linear enamel hypoplasia on teeth 11, 21, 31-32, 41 (grade I) and 16, 26 (grade II): *c.* 3 years ± 12 months.

2. Post-cranial skeleton

Rib cage: Two right ribs, either 7th and 8th or 8th and 9th show unhealed fractures sternal of the facet of the tubercle with development of pseudarthrosis (Figs. S23a-2 to S23a-8).

Fig. S23a-1
Internal lamina of the right ala major and the posterior fossa of the right occipital bone, showing porous bone formations (arrows).

Fig. S23a-2
Superior rim of the 7th and 8th or 8th and 9th right ribs with unhealed fractures sternal of the facet of the tubercle, resulting in the development of pseudarthrosis.

Fig. S23a-3
Superior rim of the 7th or 8th right rib, showing one end of the pseudarthrosis (star).

Fig. S23a-4
Inferior rim of the 7th or 8th right rib, showing one end of the pseudarthrosis (star).

Fig. S23a-5
Internal surface of the 7th or 8th right rib, showing one end of the pseudarthrosis (star).

Fig. S23a-6
Superior rim of the 8th or 9th right rib, showing the pseudarthrosis (arrow).

Fig. S23a-7
External surface of the 8th or 9th right rib, showing the pseudarthrosis (arrow).

Fig. S23a-8
Internal surface of the 8th or 9th right rib with a gap between both ends of the pseudarthrosis.

CR6:23b

A. Skeletal data

Preservation: Bone surface: severely eroded
Bone consistency: very fragile
Completeness: 5% preserved
Age: 1.5-2 years
Pars basilaris ossis occipitalis length: 21.5mm
Pars basilaris ossis occipitalis width: 24.5mm
Humerus right length: approximately 100mm
Radius right length: approximately 90mm
Ulna right length: 100mm
Sex: indeterminable

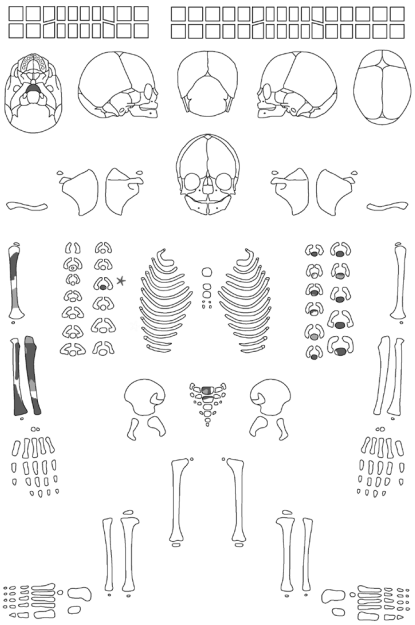

CR6:40-41a-b

Single primary Burial CG6, associated with isolated bones of at least four individuals

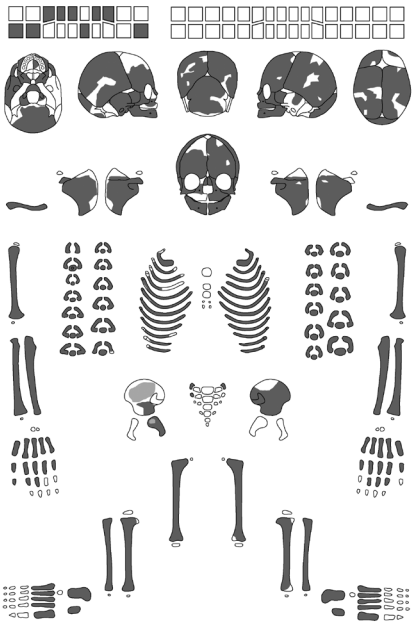

CR6:40

A. Skeletal data

Preservation: Bone surface: good
Bone consistency: relatively solid
Completeness: 100% preserved
Age: 0 years (±2 months)
Dental development
Pars basilaris ossis occipitalis length: 16mm
Pars basilaris ossis occipitalis width: 15mm
Clavicula right length: 46mm
Humerus both length: 66mm
Radius both length: 54mm
Femur right length: 77mm
Tibia right length: 67mm
Ilium left height: minimum 29mm
Ilium left width: minimum 33mm
Ischium right length: 19.5mm
Sex: indeterminable

B. Pathological data

1. Cranium and mandible

Endocranial surface: Many blood vessel impressions are visible in the area of the tubera frontalia on both frontal bones. Additionally, there are lingulate, plaque-like new bone formations that are thicker at the deepest point of the tubera and level off to the sides (Fig. S40-1). The left parietal and the occipital bones show a striated surface with small plate-like new bone formations attached to it.
Orbital roof: The lateral half of the right orbital roof shows a more severe flaky surface on its anterior side than the left orbital roof.
Orbital floor: The left orbital roof shows a more porous and flakier surface compared to the right.

2. Post-cranial skeleton

Rib cage: Flaring of the sternal ends of the 5th-8th right ribs, particularly of the 7th and 8th. The 2nd-9th left ribs show flaring at the sternal ends, with the 8th being cup-shaped (Fig. S40-2).
Proximal and distal upper limb: At the distal ventral surface of both humeri the cortical surface does not reach the rim of the epiphyseal plate (Fig. S40-3). Flaring of the distal end of the left radius, more pronounced than at the proximal end, as well as at the distal end of the left ulna.
Proximal lower limb: The proximal end of both femora is enlarged; the distal ends are missing due to postmortem processes. At the distal ventral surface of both femora, the cortical surface does not reach the rim of the epiphyseal plate.
Distal lower limb: Both proximal and distal ends of both tibiae and the distal ends of both fibulae are enlarged.

3. Probable diagnosis of selected disease types

Metabolic diseases: Flaring of the ends of the radius and ulna as well as of the sternal ends of the ribs. Enlargement of the proximal ends (distal ends are missing) of both femora as well as of the proximal and distal ends of both tibiae and fibulae.

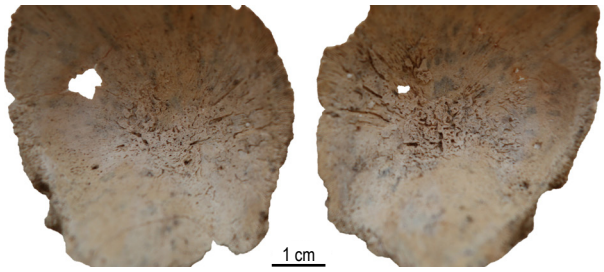

Fig. S40-1
Internal lamina of both frontal bones with lingulate, plaque-like new bone formations that are thicker at the deepest point of the tubera and level off to the sides.

Fig. S40-2
Anterior view of the rib cage, showing flaring of the sternal ends of the 5th-8th right ribs and 2nd-9th left ribs.

Fig. S40-3
Anterior view of both humeri, displaying flaring of the proximal metaphyses. At the distal ventral surface of both humeri, the cortical surface does not reach the rim of the epiphyseal plate (arrows).

CR6:41a-c

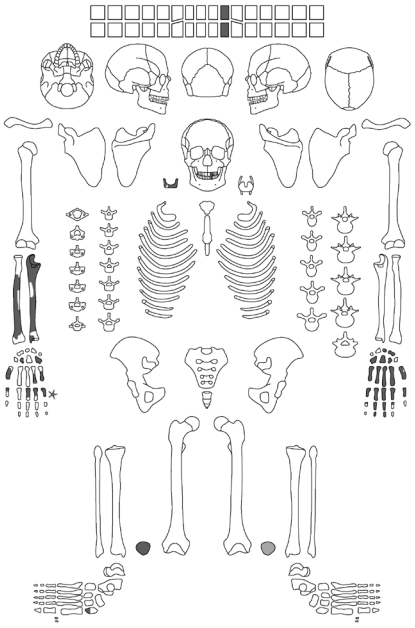

with isolated bones of minimum four individuals: at least two adults (CR6:41a), one infant (CR6:41b), one fetus (CR6:41c)

CR6:41a

Additional adult bones:
Parts of the lower right arm and hand as well as of the left hand are from the same individual (Fig. S41a-1). The bones have a severely eroded surface and are highly fragmented. They are all gracile; all joints do not show any signs of degenerative processes. On the left ulna, the surface is covered with dark grey spots, while they are darker in colour on the radius. The joint surface of the proximal end of the ulna and the surface of the distal end of the joint on the ventral side are partly destroyed by white crystals (Fig. S41a-2), which are located within the compact bone. Except for the radius, all other bones have crystals within the compact or spongy bone. The distal phalanx of the 4th digit of the left hand shows an irregular proximal joint surface with two foramina connected by a small groove (Fig. S41a-3). It might resemble a well healed fracture without any dislocation of fragments.
Isolated adult bones (Fig. S41a-4):
Fragmented rib with rodent gnawing marks.
Fragment of a right os cuneiforme I.
Os hyoideum: the left greater horn is fused with the body. The right side might have been as well but is broken postmortem.
Two single incisors, probably tooth 22 and 32 not belonging to the same individual.
Tooth 22: calculus (grade I), dental wear (grade 1).
Tooth 32: calculus (grade II), dental wear (grade 3); large enamel chipping on the distal occlusal rim.
Right and left patellae without degenerative changes of the joint surfaces, the right patella is bipartite (Fig. S41a-5).

Fig. S41a-1
Ventral/ palmar view of the lower right arm and hand, as well as the left hand.

Fig. S41a-3
Proximal joint surface of the distal phalanx of the 4th digit of the left, displaying an irregular surface with two foramina connected by a small groove.

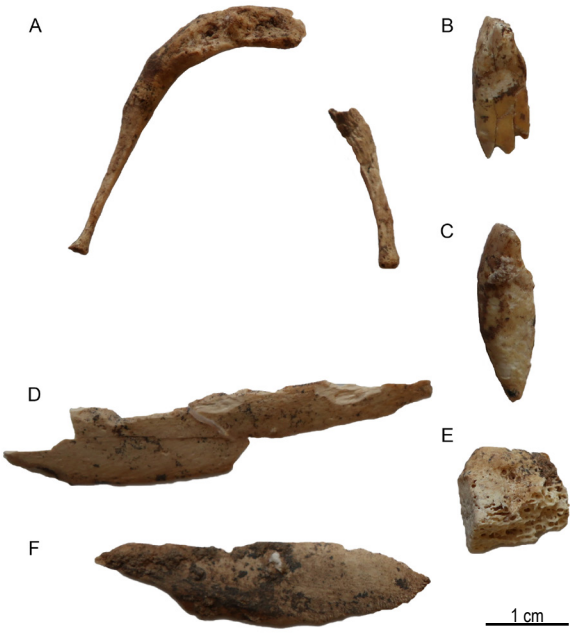

Fig. S41a-4
Isolated adult bones: *A* os hyoideum, *B* incisor, tooth 22, *C* incisor, tooth 32, *D* fragmented rib, *E* fragment of a right os cuneiforme I, *F* fragmented rib.

Fig. S41a-2
Right os trapezoideum with white crystals within the compact bone.

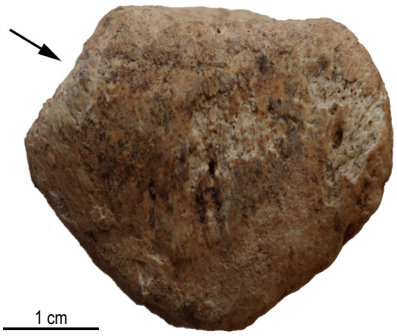

Fig. S41a-5
Anterior surface of the right patella bipartita (arrow).

CR6:41b

Additional isolated infant bones:
Os ilium right (Fig. S41b-1): width 32mm, height 30.5mm
Right upper rib (Fig. S41b-2)

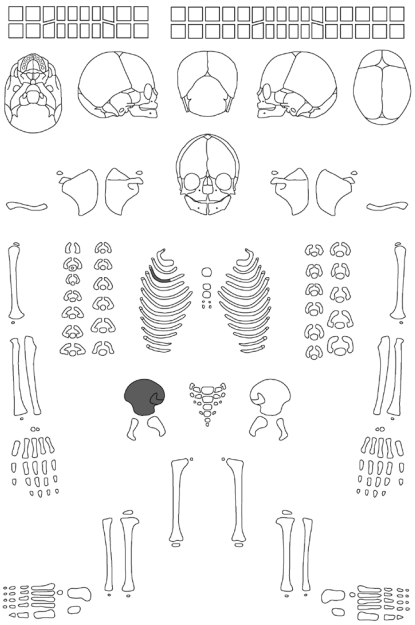

Fig. S41b-1
External surface of the right os ilium.

Fig. S41b-2
Superior rim of a right upper rib.

CR6:41c

Additional fetal bones (Fig. S41c-1)**:**
Fragment of the left radius
Fragment of the right os ilium

Fig. S41c-1
Anterior surface of a fragment of the left radius and external surface of a fragment of the right os ilium.

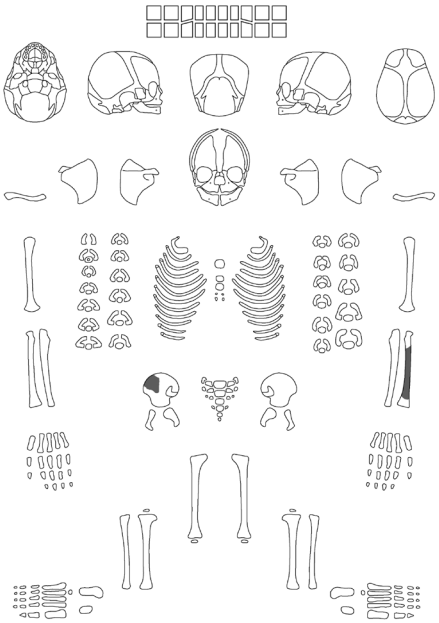

C1:46

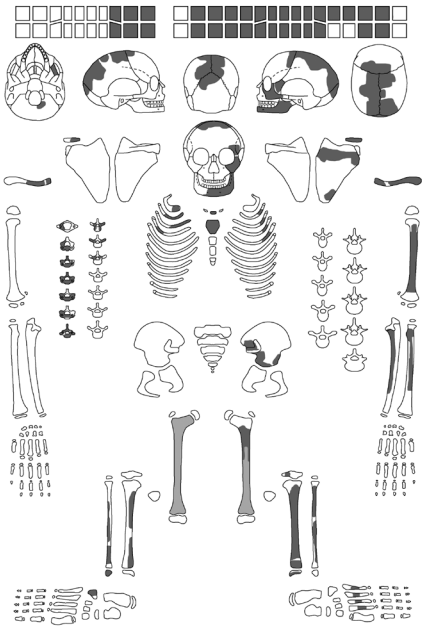

Single primary Burial CG7

A. Skeletal data

Preservation: Bone surface: severely eroded, red staining all over the bones, black spot-like colouration on long bones
Bone consistency: very fragile
Completeness: 40% preserved
Age: 8 years (± 24 months)
Dental development: 8 years (± 24 months)
Tibia left length: 195mm
Sex: female > male
Mental protuberance rather prominent, angulus roundish with no prominent muscle attachments on the sides

B. Pathological data

1. Cranium and mandible

Dentition, alveolar region, and temporomandibular joints: Deciduous dentition: calculus on teeth 53-55, 65 (grade I). Attrition of the anterior and posterior dentition (grade 3-4). Permanent dentition (partly erupted): calculus on teeth 31-32, 36, 41-42, 46 (grade I). Attrition of the anterior and posterior dentition (grade 2). Transverse linear enamel hypoplasia on teeth 11, 31-32, 42 (grade I) and 13, 17, 23, 43 (grade II): *c.* 4 years ± 12 months, 5 years ± 16 months, 6 years ± 24 months, 7 years ± 24 months. Spot-like enamel hypoplasia on tooth 25: a 3 x 3mm large shallow pit on the mesial buccal surface (Fig. S46-1). On the lingual mesial half, there is a 2 x 2mm slightly deeper irregular defect (Fig. S46-2). Tooth 24 has three very small indentations on the occlusal surface of the lingual cusp. Tooth 27 has two small foramina on the tip of both distal cusps (Fig. S46-3), tooth 17 has a small foramen on the medial cusp, tooth 15 has a small foramen on the tip of the lingual cusp.

2. Post-cranial skeleton

Shoulder girdle: Asymmetrical shape of the manubrium sterni with a convex shape of the right lateral border in contrast to the concave shape of the left border (Figs. S46-4, S46-5). The left sternal joint surface has a notch in its middle region. The left clavicle shows a depression of 26 x 2.5mm in the area of the attachment of the delta muscle.
Distal lower limb: The left tibia has a deep line at the attachment of the soleus muscle.

3. Probable diagnosis of selected disease types

Morphological variation/ developmental disorder: Asymmetrical shape of the manubrium sterni.

Fig. S46-1
Spot-like enamel hypoplasia on the mesial buccal surface of tooth 25.

Fig. S46-2
Deep irregular defect on the lingual mesial surface of tooth 25.

Fig. S46-3
Tooth 27 with two small foramina on the tip of both distal cusps.

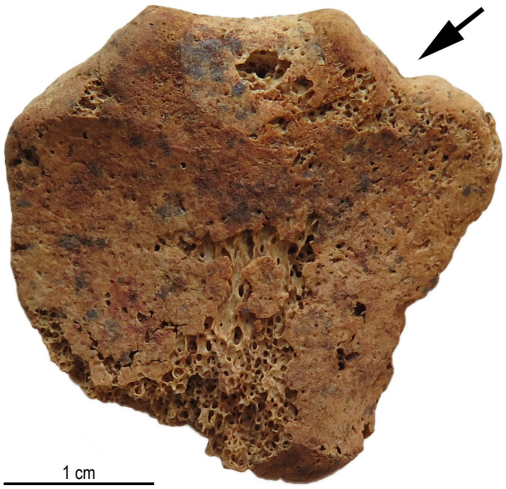

Fig. S46-4 Anterior surface of the manubrium sterni, showing a depression on the left sternoclavicular surface (arrow).

Fig. S46-5 Posterior surface of the manubrium sterni, showing a depression on the left sternoclavicular surface and red staining of the surface.

C10:405 Ind. I+II

Double Burial CG8

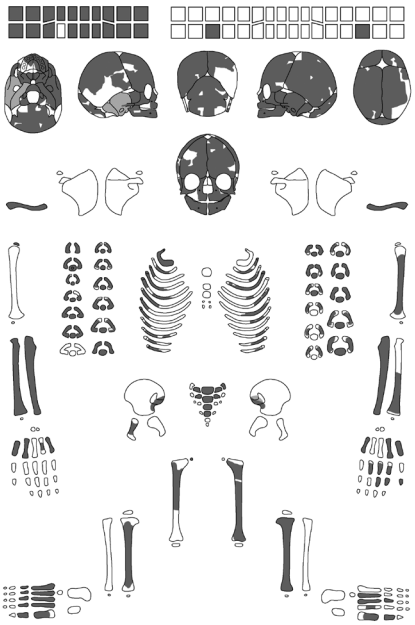

C10:405 Ind. I

A. Skeletal data

Preservation: Bone surface: moderate, few black spots
Bone consistency: fragile
Completeness: 90% preserved
Age: 6-9 months
Dental development: 9 months (±3 months)
Pars basilaris ossis occipitalis length: 19.5mm
Pars basilaris ossis occipitalis width: 21mm
Radius right length: 64mm
Femur left length approximate: 106mm
Tibia left length: 85mm
Sex: male >= female, genetic: female
Mandible rather two tubera than prominent mental protuberance

B. Pathological data

1. Cranium and mandible

Ectocranial surface: Slight porous surface on the left occipital and parietal bones at the lambdoid suture, more prominent than on the right occipital bone (Fig. S405.I-1). Sutura mendosa on the left occipital bone (Fig. S405.I-2).
Endocranial surface: The surface of both the left and right frontal bones, at their border to the anterior fossae, is covered with porous new bone formations. Similarly, the surface of the occipital bone also exhibits porous formations (Figs. S405.I-2, S405.I-3).
Endocranial surface of the cranial base: All surfaces, particularly of the medial fossae, are covered with thick layers of porous new bone formations. These formations are thicker in the lower parts of the cranial base, surrounding the foramen magnum, and between the foramen ovale and rotundum (Fig. S405.I-4).
Cranial sulci: The surface of the superior sagittal sulcus in the region of the parietal and occipital bones (Figs. S405.I-2, S405.I-3) as well as the left sigmoid sinus are covered with thick layers of porous new bone formations.
Orbital roof: Both orbital roofs have a densely porous surface, particularly at the lateral sides (Fig. S405.I-5).
Orbital floor: The surface of the right side has small blood vessel impressions and is more porous than the left side.
Nasal cavity: The surface of the floor and lateral wall on the right side is porous.
Nasolacrimal duct: The surface of the floor and lateral walls on the right side is porous.
Hard palate: The surface is porous and has a reticulated structure.
Dentition, alveolar region, and temporomandibular joints: Spot-like enamel hypoplasia on tooth 81: *c.* 7 ± 2 months in utero.

3. Probable diagnosis of selected disease types

Morphological variation/ developmental disorder: Sutura mendosa of the left occipital bone.

Fig. S405.I-1
External lamina of the left parietal bone with porous surface near the lambdoid suture.

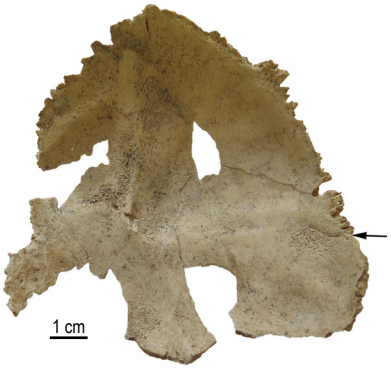

Fig. S405.I-2
Internal lamina of the occipital bone with a sutura mendosa on the left side (arrow).

Fig. S405.I-3
Internal lamina of the occipital bone covered with porous new bone formations.

Fig. S405.I-4
Internal lamina of the right pars lateralis ossis occipitalis covered with a thick layer of porous new bone formations.

Fig. S405.I-5
Right orbital roof with a densely porous surface.

C10:405 Ind. II

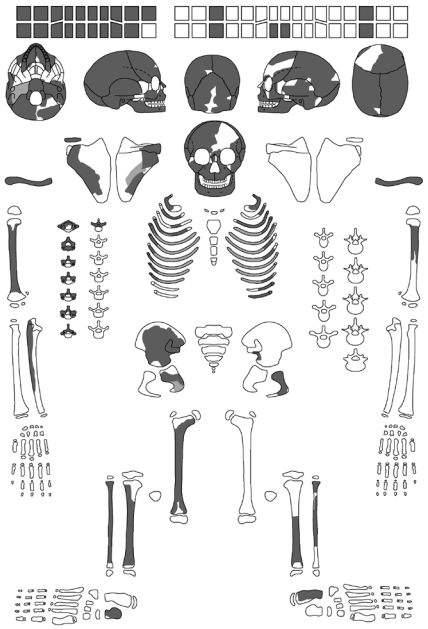

A. Skeletal data

Preservation: Bone surface: moderate, few black spots
Bone consistency: very fragile
Completeness: 80% preserved
Age: 3-4 years (dental age), 1.5-2.5 years (long bone age)
Dental development: 3-4 years
Pars basilaris ossis occipitalis length: 22mm
Pars basilaris ossis occipitalis width: 22.5mm
Clavicula left length: 60mm
Femur right length: fragment length 132mm, approximately 145mm
Femur right circumference: 41mm
Tibia right length: fragment length 100mm, approximately 117mm
Tibia right sagittal diameter at the mid-shaft: 11mm
Tibia right transverse diameter at the mid-shaft: 9mm
Os ilium right width: fragment 50, approximately 52-54mm
Sex: female > male
Mandible: prominent mental protuberance

B. Pathological data

1. Cranium and mandible

Ectocranial surface: Porous surface of both parietal bones at the lambdoid suture (Fig. S405.II-1).
Endocranial surface: On the lateral sides of both the left and right frontal bone at their border to the anterior fossae, there are shallow small roundish pit-like impressions (Fig. S405.II-2). On both parietals and the occipital bone, additional small reticulated blood vessel impressions are visible (Fig. S405.II-3). In the impressiones digitatae of both temporal bones, remodeled porous bone formations are present.
Endocranial surface of the cranial base: The occipital bone exhibits lingulate, plaque-like new bone formations next to the midline close to the foramen magnum on both sides (Fig. S405.II-4).
Cranial sulci: The right transverse sinus shows lingulate, plaque-like new bone formations in its lateral area.
Orbital roof: Both orbital roofs have a slightly porous surface (Fig. S405.II-5).
Orbital floor: The surface of the right side is porous.
Dentition, alveolar region, and temporomandibular joints: Deciduous dentition: calculus on teeth 63, 71 (grade I). Attrition of the anterior dentition (grade 2-3) and posterior dentition (grade 1-2). Small enamel chipping on distal occlusal surface of tooth 84. Permanent dentition (not yet erupted): Transverse linear enamel hypoplasia on teeth 16, 26 41, 42 (grade I): *c.* 2 years ± 1 year. Spot-like enamel hypoplasia on tooth 41.

2. Post-cranial skeleton

Proximal upper limb: The proximal quarter of both humeri is flattened (Fig. S405.II-6).
Proximal lower limb: Severe bowing of the shaft of the right femur to ventral but without deformation (Fig. S405.II-7).

3. Probable diagnosis of selected disease types

Morphological variation/ developmental disorder: Strong discrepancy between the estimated older dental age and the delayed long bone age, which could indicate stunted growth.
Metabolic diseases: enlargement of proximal ends of the metaphyses of humerus, femur, and tibia as well as bowing of the right femur could indicate rickets, although no further signs for this disease are visible.

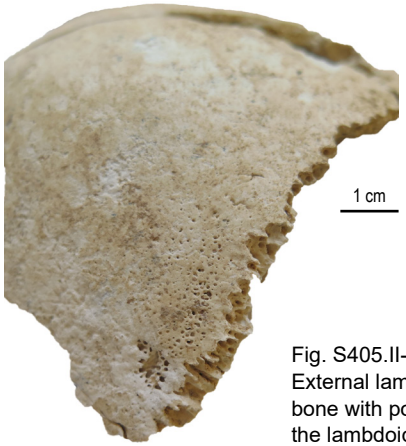

Fig. S405.II-1
External lamina of the left parietal bone with porous surface near the lambdoid suture.

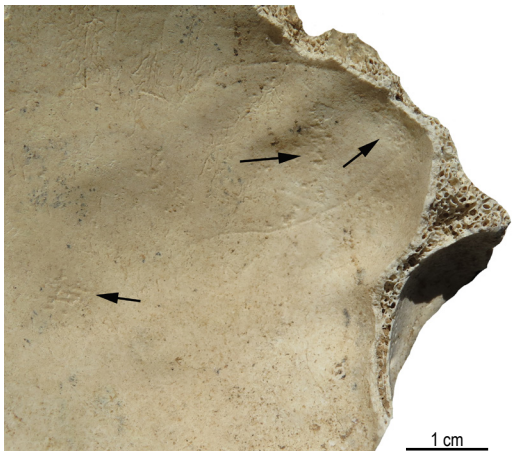

Fig. S405.II-2
Internal lamina of the right frontal bone with shallow, small roundish pit-like impressions (arrows).

Fig. S405.II-3
Internal lamina of the right parietal bone with small, reticulated blood vessel impressions (arrows).

Fig. S405.II-4
Internal lamina of the occipital bone next to the midline close to the foramen magnum with lingulate, plaque-like new bone formations.

Fig. S405.II-5
Right orbital roof with slightly porous surface.

Fig. S405.II-6
Anterior surface of the right (R) and left (L) humeri, with flattened proximal quarter in contrast to humeri of healthy individuals of the same age.

Fig. S405.II-7
Medial surface of the shaft fragment of the right femur, showing severe shortening and bowing ventrally in comparison with a left femur of an individual of the same age.

C10:408.8

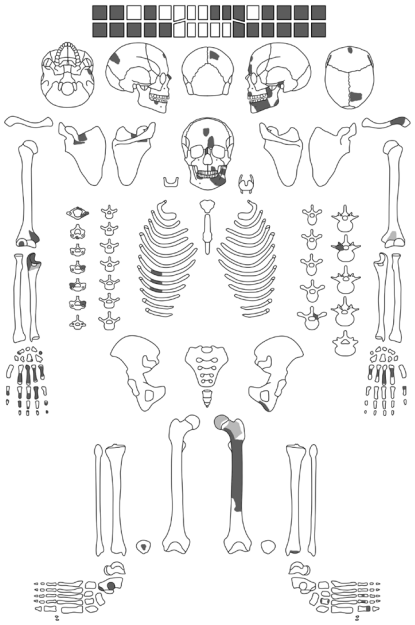

Single Burial CG10

A. Skeletal data

Preservation: Bone surface: severely eroded, many black spots, remnants of roots, rodent gnawing marks
Bone consistency: very fragile
Completeness: 5% preserved
Age: 25-35 years
Dental wear of the molars: 25-35 years
State of cancellous bone within the femoral head and neck: dense, suggesting young adult age
Sex: male >= female
prominent glabella (score 3-4) (Buikstra and Ubelaker, 1994), robust ramus mandibulae

B. Pathological data

1. Cranium and mandible

Dentition, alveolar region, and temporomandibular joints: Calculus: on all of the teeth (grade I-II). Attrition of the anterior (grade 4-5) (Fig. S408.8-1) and posterior dentition (left side: grade 2-5; right side: grade 2-3). Multiple chippings of enamel on teeth 15, 17, 18, 23, 25, 27, 36, 38, 45-48 ranging from less than 1mm to 4 x 4mm in size (Fig. S408.8-2). Transverse linear enamel hypoplasia on teeth 17, 18, 22, 23, 25, 27, 28, 33-35, 37, 38, 44 (grade II): *c.* 5 years ± 16 months, 6 years ± 24 months, 7 years ± 24 months, 12 years ± 30 months. Interproximal grooving: tooth 26: mesial surface (7 x 1mm) (Fig. S408.8-3), distal surface (5 x 1.2mm) (Fig. S408.8-4); tooth 27: lingual half of the mesial surface (4 x 1mm) (Fig. S408.8-5).

2. Post-cranial skeleton

Vertebrae: The left lower joint of the atlas shows pitting of the surface and subtle enlargement of the rim (Fig. S408.8-6).

3. Probable diagnosis of selected disease types and other features

Intentional/ unintentional modifications: Probable work-related use of the anterior teeth. Probable habitual use of toothpicks to remove fibers from the interdental spaces.

Fig. S408.8-1
Labial surface of tooth 23 with calculus, transverse linear enamel hypoplasia, and irregular dental wear.

Fig. S408.8-2
Mesial surface of tooth 23 with calculus and 4 x 4mm chipping of the enamel.

Fig. S408.8-3
Mesial surface of tooth 26 with interproximal grooving between crown and root.

Fig. S408.8-4
Distal surface of tooth 26 with interproximal grooving between crown and root.

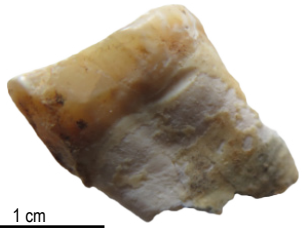

Fig. S408.8-5
Mesial surface of tooth 27 with interproximal grooving in the lingual half between crown and root.

Fig. S408.8-6
Left lower joint of the atlas, showing pitting of the surface and subtle enlargement of the rim.

CR28.2:122a-b/123a-b

Multiple primary and secondary Burial CG9[2]

CR28.2:122a

A. Skeletal data

Preservation: Bone surface: severely eroded (Fig. S122a-1)
Bone consistency: very fragile
Completeness: 30% preserved (Fig. S122a-2)
Age: 3 years (+12 months)
Dental development: 3 years (+12 months) (Fig. S122a-3)
Ulna left length fragment: 84mm
Femur right: 72-74mm
Os pubis left length: 18mm
Sex: indeterminable

Fig. S122a-1
External lamina of cranial vault bones.

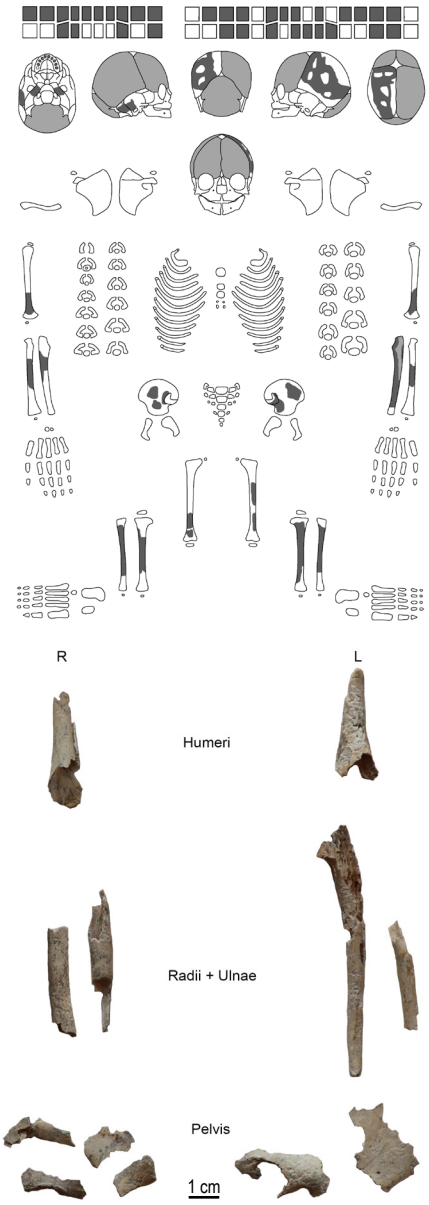

Fig. S122a-2
Fragments of long bones of the upper extremity and pelvis.

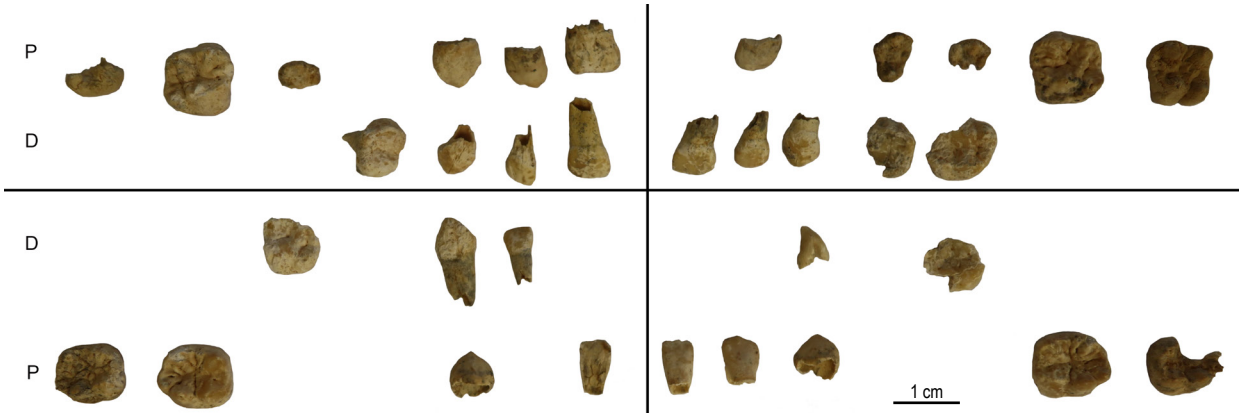

Fig. S122a-3 Teeth of the deciduous (D) and permanent (P) dentition.

[2] The skeletons of this burial are very poorly preserved, therefore, not much information can be provided.

CR28.2:122b

A. Skeletal data

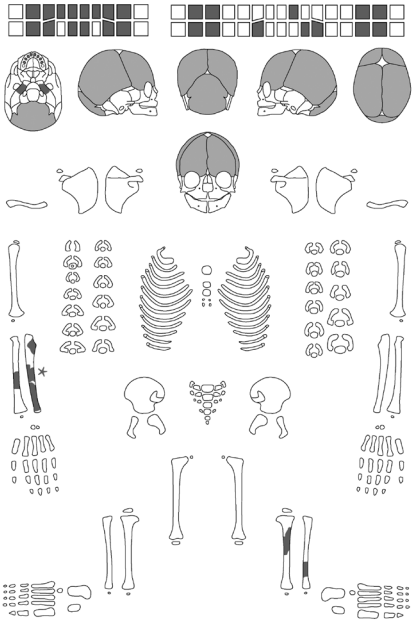

Preservation: Bone surface: severely eroded
Bone consistency: very fragile
Completeness: 5% preserved
Age: 3 years (± 12 months)
Dental development: 3 years (± 12 months)
(Fig. S122b-1)
Sex: indeterminable

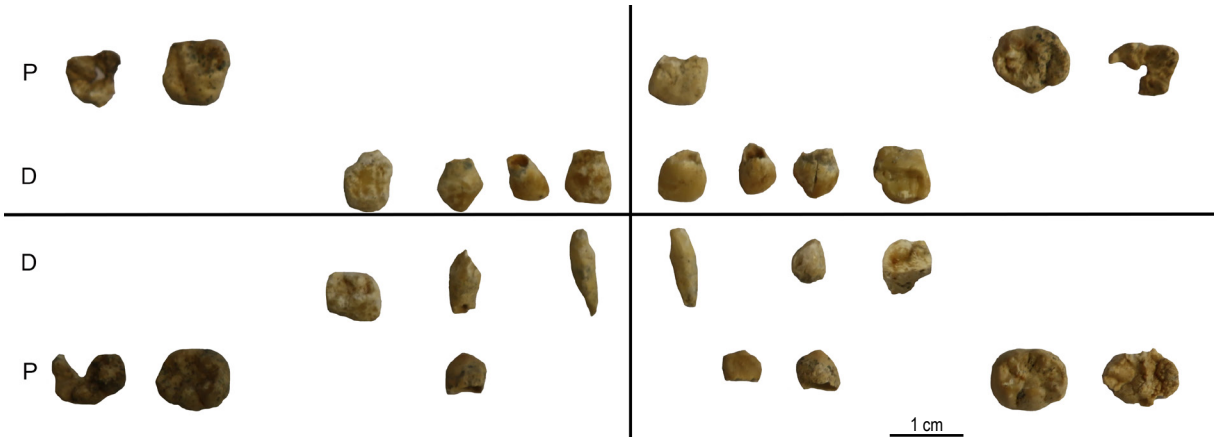

Fig. S122b-1 Teeth of the deciduous (D) and permanent (P) dentition.

CR28.2:123a

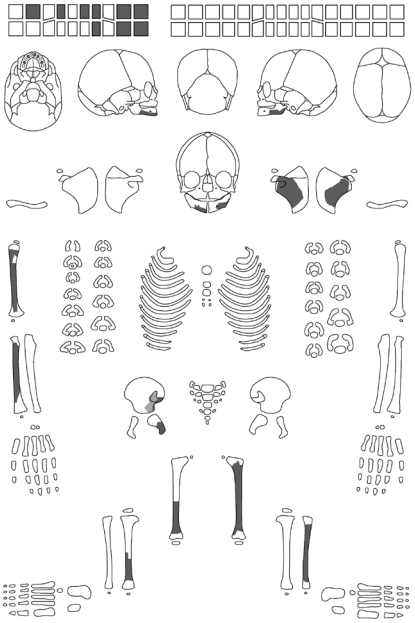

A. Skeletal data

Preservation: Bone surface: severely eroded
Bone consistency: very fragile
Completeness: 35% preserved (Fig. S123a-1)
Age: 9.5 lunar months
Dental development: 0 years (± 2 months)
(Fig. S123a-2)
Comparing the sizes of the fragmented long bones to complete fetus bones, it fits the age of 9.5 lunar months
Humerus right fragment length: 46 mm
Radius right fragment length: 39mm
Femur left fragment length: 52mm
Femur left circumference: 18mm
Sex: indeterminable

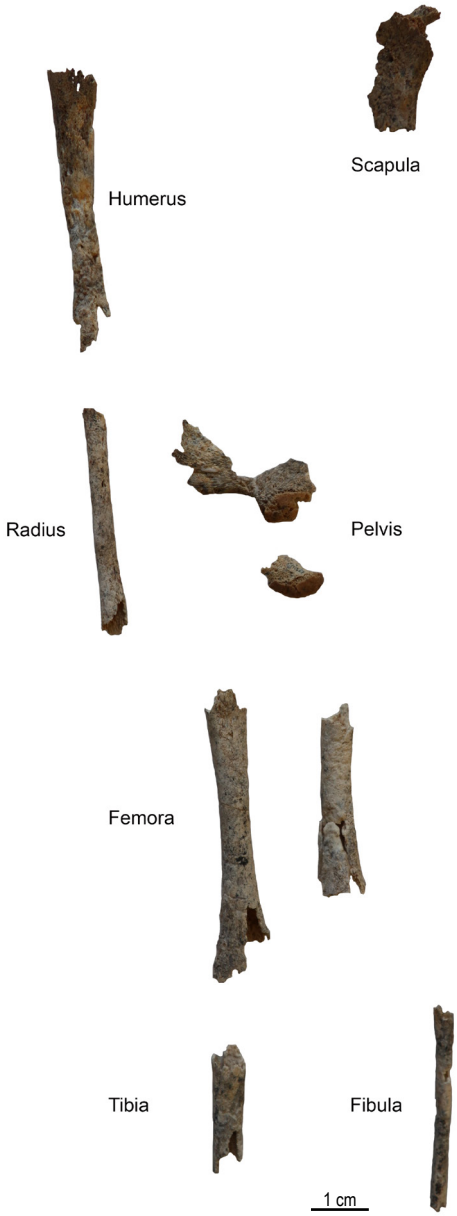

Fig. S123a-1
Anterior view of the fragments of postcranial elements.

Fig. S123a-2
Teeth of the deciduous dentition.

CR28.2:123b

A. Skeletal data

Preservation: Bone surface: severely eroded
Bone consistency: very fragile
Completeness: 35% preserved (Fig. S123b-1)
Age: 9.5-10 lunar months
Radius left fragment length: 47mm
Tibia left length: approximately 60mm
Sex: indeterminable

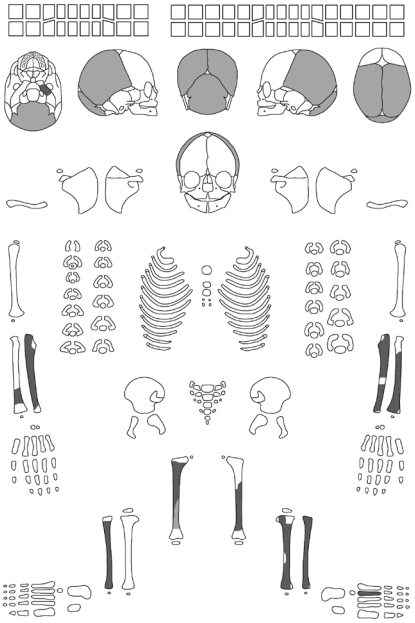

Fig. S123b-1
Anterior view of the long bones of the upper and lower extremities.

DR19:110

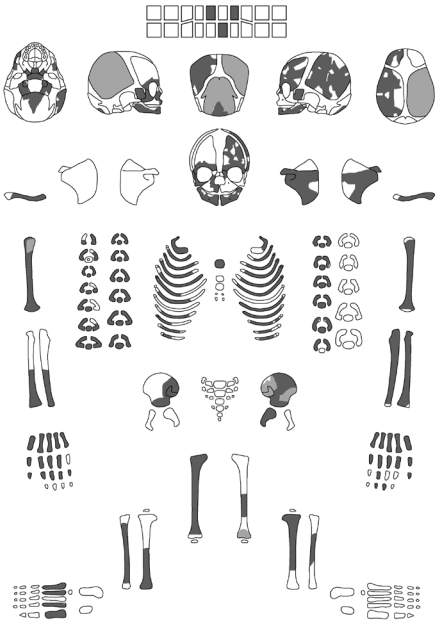

Single Burial DG2

A. Skeletal data

Preservation: Bone surface: good, but many plant roots
Bone consistency: fragile
Completeness: 80% preserved
Age: 0 years (40 weeks)
Dental development: 0 years (± 2 months)
Pars basilaris ossis occipitalis length: 15mm
Pars basilaris ossis occipitalis width: 15mm
Humerus right length: 62-63mm
Radius left length: 51mm
Femur right: 72-74mm
Os pubis left length: 18mm
Sex: indeterminable

B. Pathological data

1. Cranium and mandible

Ectocranial surface: Porous surface of the left frontal and left parietal bones, particularly severe at the cranial sutures; rather signs of bone growth than due to pathological processes. The surface of the occipital bone is widened in an area of 6 x 6mm with slight porous surface and a blood vessel impression running through this area (Figs. S110-1, S110-2).
Endocranial surface: The surface of the left frontal and left parietal from the tuber frontale, respectively parietale up to the coronal suture is covered with lingulate, plaque-like new bone formations (Fig. S110-3).
Endocranial surface of the cranial base: The surface of all fossae is porous; additionally, the surface of the posterior cranial fossa is covered with 1-2 layers of bubble-like new bone formations close to the foramen magnum.
Orbital roof: Both orbital roofs have a flaky surface, which possibly resembles physiological growth processes.
Orbital floor: The surface of the right side is slightly finely porous and flaky, resembling physiological growth.
Dentition, alveolar region, and temporomandibular joints: Only teeth 41, 52, and 61 are present.

2. Post-cranial skeleton (Figs. S110-4, S110-5)

Proximal upper limb: The proximal more than the distal ends of both humeri seem to be enlarged (Figs. S110-5, S110-6). The distal ventral surface of the right humerus is porous, which possibly resembles physiological growth. At the distal ventral surface, there are two spots in which the yellow appearance of the epiphyseal plate is visible, and they are not covered by cortical bone (Fig. S110-6).
Proximal lower limb: The proximal more than the distal end of the right femur seems to be enlarged (Figs. S110-5, S110-7). Its proximal dorsal surface is porous with fine long striations.
Distal lower limb: Both proximal and distal ends of both tibiae seem to be enlarged (Figs. S110-5, S110-8, S110-11). Its medial surface is porous, resembling physiological growth.

3. Probable diagnosis of selected disease types

Metabolic diseases: enlargement of proximal ends of humerus, femur, and tibia, *e.g.,* due to anemia.

Fig. S110-1
External lamina of the occipital bone, widened in an area of 6 x 6mm with a slightly porous surface and a blood vessel impression running through this area (*Hirox KH-870031*).

Fig. S110-2
Close-up of the lesion of Fig S110-1 (*Hirox KH-870031*).

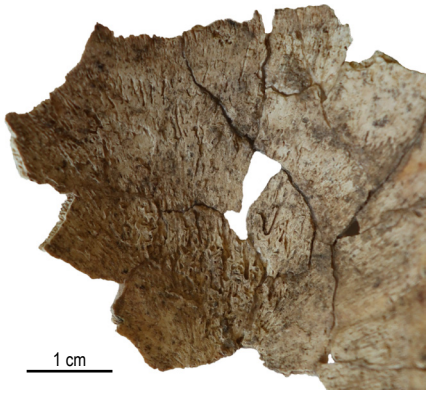

Fig. S110-3
Internal lamina of the left parietal bone in the area of the tuber parietale, covered with lingulate, plaque-like new bone formations.

Fig. S110-4
Anterior view of the preserved postcranial elements.

Fig. S110-5
Radiograph of postcranial elements in an anterior-posterior view, 60kV 4min, 3mAs.

Fig. S110-6
Anterior surface of the right humerus, exhibiting flaring of the proximal metaphysis and two areas not covered by cortical bone (arrows).

Fig. S110-7
Anterior surface of the right femur, showing flaring of the proximal metaphysis.

Fig. S110-8
Anterior surface of the left tibia, showing flaring of the proximal metaphysis.

Fig. S110-9
Flaring of the proximal metaphysis of the left tibia.

Fig. S110-10
Posterior surface of the right tibia, showing flaring of the distal metaphysis.

Fig. S110-11
Flaring of the distal metaphysis of the right tibia.